Pair driven IR fluorescence quenching of Yb^{3+} in ZrO_2:Yb^{3+}

By

Lic. Luis Octavio Meza Espinoza

2 0 0 6

For the Degree of

MASTER DEGREE IN SCIENCE (OPTICS)

Adviser

Dr. Luis Armando Diaz Torres

León Guanajuato, México

December 2006

Contend

Chapter two: Non radiative Energy transfer in crystals.

1. Introduction

2. Fundamentals of non-radiative energy transfer.

3. Rate Equation Analysis for Non Radiative Energy transfer: The General Energy Transfer Master Equations (GETME).

4. Energy transfer among two energy level ions Revisited: The Non Linear General Energy Transfer Master Equations (NLGETME)

5. Non radiative energy transfer between two and three level ions The General Energy Transfer Upconversion Equations (GETUPE):

Chapter three: Yb^{3+} dimers as quenching centers in ZrO_2:Yb^{3+} nanocrystals.

1. Introduction

2. The Yb dimers in ZrO_2.

2.1 Nanocrystal size and phase effect on Donor and acceptor concentration.

2.2 Nanocrystal size effect on Donor effective Life time.

3. Quenching simulation

Chapter four: Conclusions and Prescriptive

Appendix A

Appendix B

Agradecimientos

Para mis padres, José Meza y Juanita Espinoza por su amor incondicional, sin su ayuda nunca habría tenido los logros que he tenido.

Siempre es un privilegio y placer expresar mi gratitud a mi esposa Susana por su amor, apoyo y aliento espiritual durante la escritura de esta tesis.

Quiero agradecer a los revisores de esta tesis, cuyos comentarios detallados fueron de enorme ayuda:

Dr. Luis A Diaz-Torres
Dr. Alexander Kiriyanov
Dr. Barbosa García Oracio C.
Dr. Luis Arevalo

Agradezco de todo corazón a mis compañeros y amigos del CIO, sobre todo a David Solís, Víctor Romero, Héctor Arellano Y Joshua Del Valle por su apoyo y animo, durante y después de la escritura de esta tesis. Estoy igualmente en deuda con Guillermina Muñiz y Laura González por su ayuda incondicional. Un agradecimiento a Elder de la Rosa por enseñarme a usar el quipo y por sus valiosos consejos.

Tengo una gratitud especial a mi casa de estudios la Universidad de Guadalajara de la cual me ciento orgulloso de pertenecer.

Finalmente quiero agradecer CONACYT por darme la oportunidad de continuar mis estudios en el CIO. Este proyecto fue apoyado por el CONACyT 43168-F, 46971-F.

La vida es una comedia para aquellos que la piensan y una tragedia para aquellos que la sienten.

Horace Walpole

Preface

Fluorescence quenching is a phenomena consisting in the reduction of quantum efficiency luminescence of a phosphor as the fluorescent (active) ions increase in concentration within the phosphor. That is quantitatively observed as a reduction on the lifetime of the fluorescence emission as the ion concentration increases. It turns out that the lifetime is one of the most important parameters on solid state laser optimization. So it is very important to solve this complicated problem. If we are able to understand and reproduce the behavior of the nonradiative energy transfer processes responsible of the rare earth's lifetime quenching, we could predict the behavior of the lifetime and its dependence on dopant concentration. That is, we can establish a strategy to dopant optimization in the active medium. This process up to now is in their majority, handled on a test and error strategy. Experimentalists manufacture several solid state laser material samples, doping them with several concentrations, and then undergo the photoluminescent characterization of each sample in order to find which the best is.

One of the traditional tools to study the dopant concentration quenching in a dielectric crystal, it is by means of solving the General Energy Transfer Master Equations (GETME) that govern the dynamics of the excitation energy among the active ions within the crystal. The GETME up to now had been applied only for the unlikely case in which the energy levels of the ions inside the crystal are in resonance. In addition all the involved ions are considered to have only two energy levels (one ground state and one exited state). These two considerations are nowadays supposed to fairly represent the real luminescent systems, and by solving the GETME under such assumption one can solve the concentration quenching problem. If we consider the most likely non resonant case of the energy levels, and if we increase the number of energy levels of the ions (one ground state and more than one exited state), the GETME become a non linear system. The nonlinearity of the new system, NLGETME, is a very complicated problem to solve, likewise, the number of coupled differential equations of the system increase considerably for each new added

excited level of the ions. To reduce the complexity of the NLGETME, we propose a linear approach based on the Taylor theorem. Then if we are able to solve NLGETME, we could predict what dopant concentrations are ideal without the necessity of generate so many samples.

One of the simplest luminescent ions is the rare earth Yb^{3+}, which actually have only two energy levels. Yb^{3+} ions are commonly used to enhance the absorption cross section of Er^{3+} or Tm^{3+} in several luminescent materials, with the consequent increment of the quantum efficiency of such ions under IR pumping. The trivalent Yb^{3+} ion is an effective sensitizing ion for several reasons. Yb^{3+} has only one exited 4f level, lying $10000cm^{-1}$ above the ground state, so quenching of high energy levels of the codopants by energy transfer to Yb^{3+} is not as likely as with ions having more high energy levels. It offers several very attractive features, in particular an unusually broad absorption band that stretches from below 850 nm to above 1070 nm.

Besides, it has been reported that ytterbium doped phosphors had visible emission. This visible emission was first observed and explained Nakazahua by means introducing a third virtual excited level. Recent new evidence show that this supposed virtual level is in fact a real energy level, created by the formation of a Yb-Yb pair, and it can be considered as a new entity inside in the crystal. Thus, we have two types of active fluorescent entities: isolated Yb ions having two energy levels, and Yb-Yb pairs (or dimers) that have three energy levels. Therefore Yb ions in crystals constitute the simplest system to proof if the solutions to the NLGETME can explain the fluorescence quenching of the isolated Yb ions and its dependence on the Yb ions concentration. Besides, it is possible that the solutions of the NLGETME give an adequate prediction of the visible luminescence of the dimers in the visible.

Due to the complexity of the NLGETME equations and to the great computation requirements for solve the NLGETME, it was considered that the first excited energy level of the dimmers is always excited. Thus, both the Yb isolated ions and the dimers can be considered as entities with two energy levels. Such a consideration prevents us to see what

happened with the visible emission coming out from the Yb-Yb pairs, and limits us to the Quenching in IR fluorescence as a consequence of energy transfer to the excited Yb dimmers. The Cooperative Upconversion emission of $ZrO_2:Yb^{3+}$ nanocrystals is much higher than that recently reported in $YAG:Yb^{3+}$ nanocrystals. In addition, recently $ZrO_2:Yb^{3+}$ has been reported as a very promising host for efficient photoluminescent applications. Besides, Zirconia is easy to produce by sol-gel and coprecipitation methods in our Materials Laboratories. That is the reason why we are interested in this promising crystal doped whit Yb^{3+}.

In the chapter 1 we will discuss the concentration quenching of luminescence in general. Also we review the basic ytterbium spectroscopy, as well as cooperative Yb emission. Our experimental observations on the quenching of the IR emission of Yb as well as the visible cooperative photoluminescence are presented.

NLGETME and GETME theoretical models are developed in chapter 2, two cases we will be taken, (1) donors and acceptors having two energy levels and (2) donors with two energy levels and acceptors with three energy levels. Resonant and off resonance conditions are discussed. To reduce the complexity of the NLGETME, we propose a linear approach based on the Taylor theorem.

In the chapter 3 we present the simulations results using NLGETME and GETME, and we approach the Yb^{3+} quenching problem by considering the construction of dimers as the quenching centers in nanocrystalline $ZrO2:Yb^{3+}$. Also we discuss the nanocrystal size and phase effect on Donor and acceptor concentration and effective Donor Life time.

In the chapter 4 we present conclusions of this work. We have three notable results, (1) we are able to reproduce concentration quenching of Yb ions using the Yb dimmer approach; (2) the NLGETME simulations and the dimer construction lead to observe the donor lifetime dependence on crystallite size; and (3) the nonresonant energy levels between ions is a important parameter that could become an important issue for high concentrations of dopants. At the end of Chapter 4 we indicate some of the immediate perspectives for the continuity of the present work.

Chapter 1:

Quenching of the IR emission of Yb^{3+} in ZrO_2

1. Introduction

In general, with increasing doping concentration the distances between active ions decrease and in consequence interaction among active ions will increase leading to concentration quenching. Thus the lifetimes of upper level decrease. Usually, the concentration quenching may occur through the following channels: (1) Cross-relaxation among active ions, (2) non radiative transfer of energy among active ions and in the end transfer to a quenching centers, (3) interaction between active ions and host resulting in transfer to energy lattice defects, (4) direct energy transfer to quenching centers such as color centers, OH^- radicals, electron and hole vacancies, etc. Experimental evidence shows that concentration quenching in Yb-doped laser host may occur through Upconversion to co-dopants such as Er^{3+}, Tm^{3+}, Dy^{3+}, Mn, Cr, etc. Such phenomenon is considered a deleterious process for the 1.04 micron emission of Yb3+. But, on the other side it is an advantage when one is looking for new visible emitters. Another interesting quenching mechanism is the cooperative upconversion process in which it is assumed the emission of a visible photon thanks to the simultaneous de-excitation of two excited Yb^{3+} ions, so called a Yb^{3+} pair or YB^{3+} dimer. Takugo Ishii proved theoretically the viability of such a Yb^{3+} pair and its absorption and emission probabilities [1]. So, in this thesis we focus on the IR fluorescence of ZrO_2:Yb^{3+} and its quenching. We address the Yb^{3+} pair topic as an approach to clarify the nature of the cooperative upconversion and its relationship with the Yb^{3+} IR fluorescence quenching. Thus, the concentration quenching in ZrO_2 crystals with high Yb^{3+} doping levels is studied and a plausible explanation is given.

2. The concentration quenching of luminescence

In principle, an increase in the concentration of a luminescent center in a given material should be accompanied by an increase in the emitted light intensity, this being due to the corresponding increase in the absorption efficiency. However, such behavior only occurs up to a certain critical concentration of luminescent centers. Above this concentration, the luminescence intensity starts to decrease. This process is known as concentration quenching of luminescence.

In general, the origin of luminescence concentration quenching lies in a very efficient energy transfer among the luminescence centers. The quenching starts to occur at a certain concentration, for which there is sufficient reduction in the average distance between these luminescence centers to favor energy transfer [2]. Due to very efficient energy transfer, the excitation energy can migrate about a large number of centers before being emitted. However, even for the purest crystals, there's always a certain concentration of defects or trace ions that can act as acceptors, so that the excitation energy can finally be transferred to them. These centers can relax to their ground state by multiphoton emission or by infrared emission. Thus, they act as energy sink within the transfer chain and so the luminescence becomes quenched, as illustrated in Fig. 1a. These kinds of centers are called "killers or quenching traps".

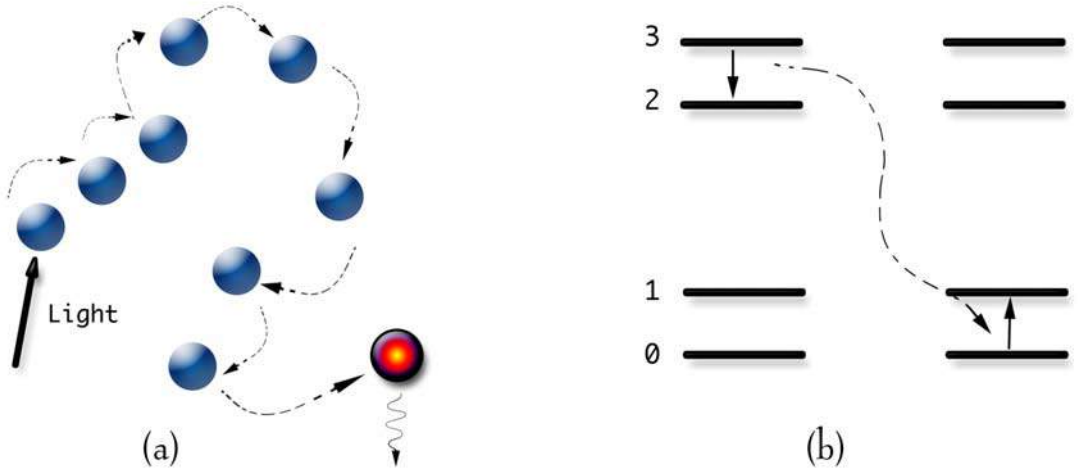

Fig 1 (a) Schemes of possible mechanisms for luminescence concentration quenching: Migration of excitation along a chain of donors (circles) and a killer (red circle), acting as non radiative sink. (b) Cross relaxation

Concentration quenching can also be produced without actual migration of the excitation energy among the luminescence centers. This occurs where the excitation energy is lost from among the emitting state via "cross relaxation" mechanism. This kind of relaxation mechanism occurs by resonant energy transfer between two identical adjacent centers, due to the particular energy level structure of these centers. Figure 1b shows a simple possible energy-level scheme involving cross-relaxation. We suppose that for isolated centers radiative emission ($3 \rightarrow 0$) from level 3 is dominant. However, for two nearby similar centers a resonant energy transfer mechanism can occur in which one of the centers (the excited one, acting as the donor) transfer part of its excitation energy –for instance (E3-E2)- to the other center (the non excited one, acting as the acceptor) exciting it whit an energy (E1-E0) that in turn is equal to (E3-E2). This resonant transfer becomes possible due to the particular disposition of the energy levels, in which the energy for the transition $3 \rightarrow 2$ is equal to that for transition $0 \rightarrow 1$. As results of the cross relaxation, the donor center will end excited in state 2 while the acceptor center will reach the exited state 1. After the non radiative transfer, these states undergo a non radiative relaxation or emission of photons with energy other than $E_3 \rightarrow E_0$; in any case the $3 \rightarrow 0$ emission will be quenched.

As the concentration quenching results in the depopulation of the emitting level, the decay time of such excited level is reduced each time an energy transfer process takes place. In general, this decay-time reduction is much easier to measure experimentally than the reduction in population of excited levels. In fact, the easier way to detect luminescence concentration quenching is to analyze the lifetime of the excited centers as a function of the concentration. The critical concentration is then the concentration for which the lifetime starts to be reduced.

3. Ytterbium Basic Spectroscopy

Ytterbium is one of the most versatile laser ions in solid state laser host [3]. It offers several very attractive features, in particular an unusually broad absorption band that stretches from below 850 nm to above 1070 nm because of the $^2F_{7/2} \rightarrow {}^2F_{5/2}$ transition, as illustrated with a representative absorption spectrum in Figure 2. Yb-doped host can thus be pumped with a wide selection of solid-state or semiconductor

lasers, including: AlGaAs ($\sim 800-850nm$) and InGaAs ($\sim 980nm$) laser diodes, Nd:YLF (1047 nm) and Nd:YAG (1064 nm) lasers. This broad pump band also relaxes considerably both the requirements for specific pump wavelength and its stability with temperature. Just as importantly, Yb fluoresces effectively over an equally impressive range, from approximately 970 to 1200 nm (see Fig. 2). This is broader than the range available from Nd-doped host Lasers, which is one of the attractions of Yb^{3+} over Nd^{+3}. The Yb-doped fiber laser, therefore, can generate many wavelengths of general interest: for example, for spectroscopy or for pumping other Lasers and amplifiers [3].

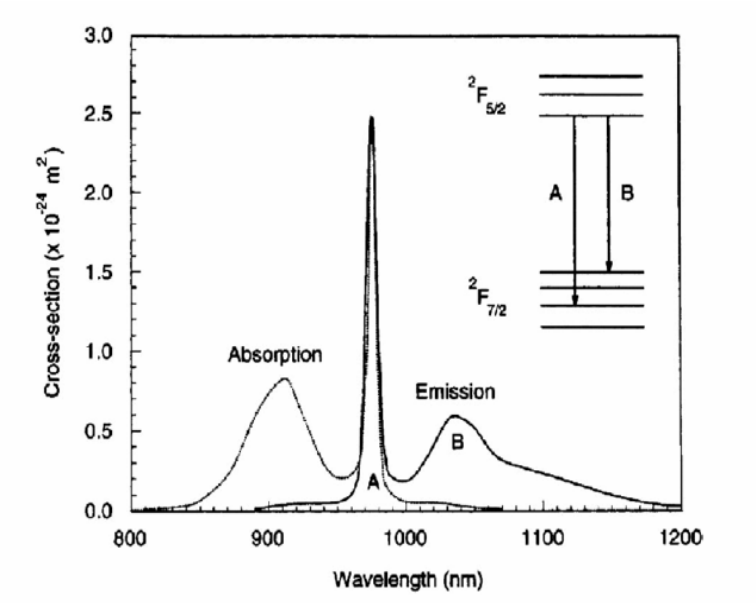

Fig 2. Ground-state absorption spectrum, emission spectrum and energy level diagram of Yb^{3+} in silica. The solid lines identify the radiative transitions responsible for the two features in the emission spectrum.

Another well-known advantage of Yb^{3+} is the simplicity of its energy level diagram. As illustrated in the inset of Figure 2, Yb^{3+} exhibits only a ground state ($^2F_{7/2}$) and a metastable state ($^2F_{5/2}$) spaced by approximately $10,000cm^{-1}$. The radiative lifetime of the $^2F_{5/2}$ state is typically in the range of $700-1400\ \mu s$, depending on the host [4]. The absence of higher energy levels greatly reduces the incidence of multi-phonon relaxation and ESA (excited-state absorption) and, therefore, should facilitate the development of high-power lasers. Yet another benefit is the abnormally high absorption and emission cross sections of Yb, which are typically several times higher than in multicomponent glasses. These combined features allow for very strong pump

absorption and very short cavity lengths (or host length) as in the case of the Disk configuration high power Yb^{3+} lasers [3, 5, 30]. A Yb-doped laser is typically pumped into the higher sublevels of the ${}^2F_{5/2}$ manifold (see inset of Fig. 2). At wavelengths below about 990 nm, it behaves as a true three-level system (transition A in Fig. 2), whereas at longer wavelengths, from 1000 to 1200 nm (transition B), it behaves as a quasi-four-level system.

The special electronic configuration of Yb^{3+} makes the 4f electrons less shielded than in other ions of the lanthanide series, showing higher tendency to interact with neighbor ions. Such interaction is not restricted to different ion. It has been reported that Yb-Yb pair interaction produce visible emission [6]. That is, when there is neither an intermediate nor a final energy level (from the co-dopant) to be populated in order to emit in the visible. Such emission is named cooperative upconversion (CUC) and was first observed by Nakazawa in $YbPO_4$. In this case, two excited Yb^{3+} ions decay simultaneously to the ground state, whit the subsequent emission of a photon with the double of energy. This process has been reported for different materials in bulk as a weak signal, but recently it was been reported strong CUC emission in both fibers and nanosized phosphors [7, 31], and the general assumption is that the enhanced emission is due to nanosized confinement effects.

4. Cooperative transitions of the Yb^{3+} dimer

The trivalent ytterbium (Yb^{3+}) dimers in crystals have been considered a good system to investigate cooperative transitions [6, 1]. The usual assumption is that the energy structure is simple, analogous to that of a free Yb^{3+} ion having only two levels ($2F_{7/2}$ and $2F_{5/2}$) split by spin–orbit interaction. Absorption and emission in the green region could be roughly attributed to the simultaneous transitions of the two Yb^{3+} ions that conforms the dimer. The first observation was reported by Nakazawa and Shionoya in $Yb^{3+}:YPO_4$ [6]. A frequently studied material has been $Yb^{3+}:CsCdBr_3$ Goldner et al. calculated the transition probability of cooperative emissions [8]. The theoretical concept in those works was based on the Dexter model [32]. Further detailed discussion concerning the type of pairs (although still controversial) used a different

phenomenological method, which was also based on an isolated ion model [9]. The sense of "dimer molecule," instead of the isolated two-ion model, was directly considered by Hehlen and Güdel, who used a notation $Yb2Br_{9.}^{3-}$ in the $Cs_3Yb_2Br_9$ crystal [10]. Their experimental work covered not only the well-studied cooperative emission transitions but also the absorption $(2F_{5/2}2F_{5/2}) \rightarrow (2F_{7/2}2F_{7/2})$ ones too, and the cooperative transition probabilities were estimated. A direct discussion on the relation between chemical bonds and cooperative transition probability is seen in an earlier work by Schugar et al [11]. They insisted that covalency played a much more important role than interionic distances, the only parameter in the Dexter model to discuss the difference among different crystals. The relation between covalency and transition probability is the key to allow material design, but the number of studies analyzing this relation is quite small due to the high degree of complexity reached when taking in to account chemical bonding.

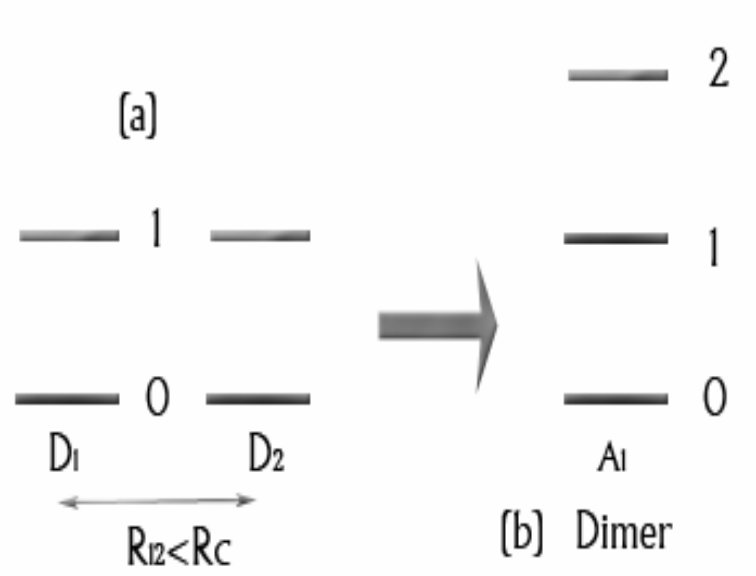

Fig 3 (a) A dimer is formed when the distance between an i-th ion Yb and a j-th ion Yb is smaller at a critic distance. (b) One dimer has three levels of energy.

The customary consideration for Yb dimer constitution is that two Yb ions are close enough so their electronic wavefunctions overlap. A new approach was recently proposed by Takugo Ishii [1]. In his work a Yb dimer is constituted of two Yb ions and a bridging Oxygen. So the cooperative transition results from the overlap of the 4f orbital of Yb ions trough the 2p orbital of the bridging oxygen. His work shows that cooperative transitions occur via the $4f-2p$ overlaps between the Yb and O atoms. As

a result of this overlap, the resulting entity Yb-O-Yb has a three level energy structure, where the higher level corresponds to the cooperative transitions. And of course the intermediate level corresponds to the situations in which only one of the Yb ions whiting the dimer is excited. Also he shows that the stronger covalency in Y_2O_3 crystal, originating from the smaller coordination number, produces a stronger cooperative transition probability than the one for the case of *YAG* crystal. Based on these results; from now on we consider (as in Fig. 3) the Yb^{3+} with a structure of two energy levels, the ground state $^2F_{7/2}$ (denoted with number 0) and its excited state $^2F_{5/2}$ (denoted by 1). In consequence the dimer configuration becomes the one shown in fig. 3: The upper level $\{2F_{5/2}2F_{5/2}\}$ (level 2) that corresponds to situation in which both Yb^{3+} within the dimer are excited; the lower-energy region (level 1) is a single-particle excitations in which only one ion within the dimer is excited; and the ground state (level 0) in which both Yb^{3+} ions within the dimer are unexcited (in its single ion ground state).

Transition between these new energy levels (0,1, and 2) are originally forbidden cooperative transitions. The cooperative absorptions are transitions from the $\{2F_{7/2}2F_{7/2}\}$ configuration (level 0) to the $\{2F_{5/2}2F_{5/2}\}$ (level 2). Once we have set the dimer absorption, we can obtain the emission transitions by doing the differences between levels.

It was also absorbed that the cooperative absorption spectra is in well agreement with the self-convolution $\int f_{IR}(v) f_{IR}(E-v)\,dv$, of the IR absorption [33].

If we make the Yb absorption spectrum self-convolution, we can find the dimer spectrum approach as shown in the figure 4a. For example, if we make the IR absorption spectrum self-convolution in ZrO_2:2%Yb crystal host (see fig 4a), we can find the cooperative absorption centered at 21.3 cm^{-1} (469nm) This peak corresponds to the upper energy level $\{2F_{5/2}2F_{5/2}\}$ (level 2) of the dimer. The peak corresponding to the energy level 1 of the dimer ($\{2F_{7/2}2F_{5/2}\}$) is centered at 11.1 cm^{-1} (901nm). Besides, we can see in the figure 4a the experimental absorption spectrum; the self-convolution predicts more or less the experimental absorption spectrum.

On the other hand, we can predict the cooperative emission doing the IR emission

spectrum self-convolution (see fig 4b). The cooperative transition $(2F_{5/2}2F_{5/2}) \rightarrow (2F_{7/2}2F_{7/2})$ leads to the visible emission centred at 19.7 cm^{-1} (507nm). The transitions $(2F_{7/2}2F_{5/2}) \rightarrow (2F_{7/2}2F_{7/2})$ and $(2F_{5/2}2F_{5/2}) \rightarrow (2F_{7/2}2F_{5/2})$ lead to the IR emission centred at 10.2 cm^{-1} (980nm).

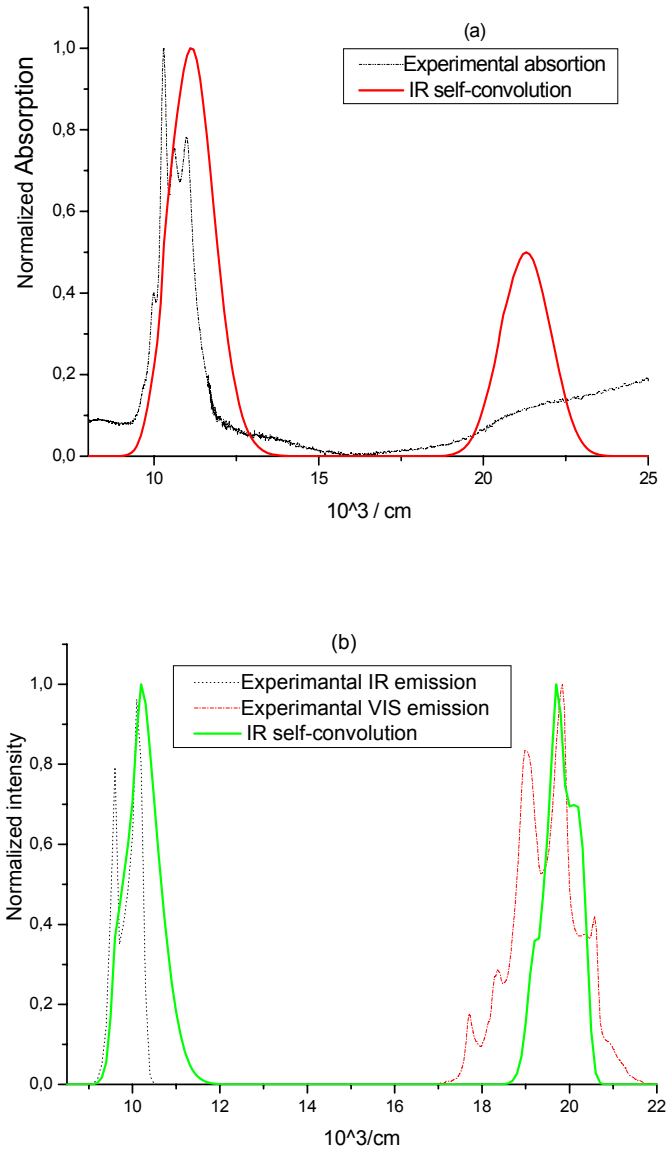

Fig. 4 (a) Yb absorption spectrum self-convolution and experimental absorption (b) emission spectrum self-convolution

5. Concentration quenching in $ZrO_2:Yb^{3+}$.

One of the most important non-radiative processes that every material shows is the multiphonon relaxation by the vibration bands of the system. When the frequency of this vibration band increases the non-radiative decay rate increases that in turn will reduce the quantum efficiency. The stretching frequency of ZrO_2 matrix is about 470 cm^{-1}, that is very small compared to that of other hosts. This low phonon energy opens up the possibility of higher efficient luminescence of active ions incorporated into ZrO_2 matrix. Furthermore, due to its superior hardness, high refractive index, optical transparency, chemical stability, photothermal stability, high thermal expansion coefficient, low thermal conductivity and high thermomechanical resistance, it can be used in a variety of photonics and industrial applications [12].

Considerable amount of work has been reported on the mechanical, physical and luminescence properties of ZrO_2. The reported results on the optical studies include the photoluminescence of sol-gel derived amorphous and tetragonal crystalline phase thin films of $ZrO_2:Eu^{3+}$, Tb^{3+}, Sm^{3+} systems [13-14]. Bulk zirconium oxide has been grown by the Skull method and cubic doped samples have been characterized [15]. More recently, the interest in the nanosized version of this rare earth doped nanophosphor has been increased. Electrons confinement effect is not expected due the localization of electrons in atomic orbital of active ions. However, excitation dynamics is influenced by the nanoscopic interaction and has been reported a dependence of the luminescence efficiency with particle size [16,17]. The interest on this new rare earth doped nanophosphor is to produce visible emission for application such as solid state lighting, displays and new generation television screen. Visible emission can be obtained under IR pumping by upconversion processes [18]. This is an interesting approximation considering that IR source is a well developed technology. Using this approximation it is possible to obtain white light for solid state lighting but new nanophosphors with high upconversion efficiency and emission if the basic colors are obtained. The emission of this kind of nanophosphors is based in two photon absorption process and also finds application in biomedicine [20]. Recently, was also reported visible emission by upconversion process in $ZrO_2:Er^{3+}$ nanophosphor pumped at 967 nm [22,23].

Nanocrystals doped with 0.5, 1.0, 2.0, 4.0, 8.0, and 12.0 mol% of Yb_2O_3 were prepared by using the sol-gel method. The samples were obtained mixing zirconium *n*-propoxide (70%), ytterbium chloride (99.99%), ethanol, hydrochloric acid, nitric acid and water. The samples were aged at room temperature, dried at 120 °C for 24 h after gelation and annealed at 1000 °C for 10 h. A detailed explanation of sample preparation was reported elsewhere [27].

The crystalline structure and crystallite size of the samples was investigated by X-ray diffraction (XRD). The crystalline phase of ZrO_2:Yb^{3+} nanophosphor is determined by the Yb concentration, see Fig. 5. At Yb_2O_3 concentrations lower than 1.0 the crystalline phase is almost monoclinic and starts to be transformed to tetragonal as the dopant concentration increases. For 2 mol% of Yb_2O_3, the main crystalline phase is tetragonal but monoclinic is still present. The small peak marked (→) correspond to the main peak of the monoclinic structure. Pure tetragonal and cubic phase was obtained for 4 and 8 mol% doped sample, respectively. The average particle size obtained from XRD pattern using the Scherrer equation was ~50 nm. Both crystalline structure and crystallite size was confirmed with TEM and HRTEM, respectively, see Fig. 6. Well faceted individual nanocrystals were observed although agglomeration was present as consequence of the high annealing temperature. HRTEM confirm that the Yb^{3+} ion content not affects the particle size but affect the crystalline structure.

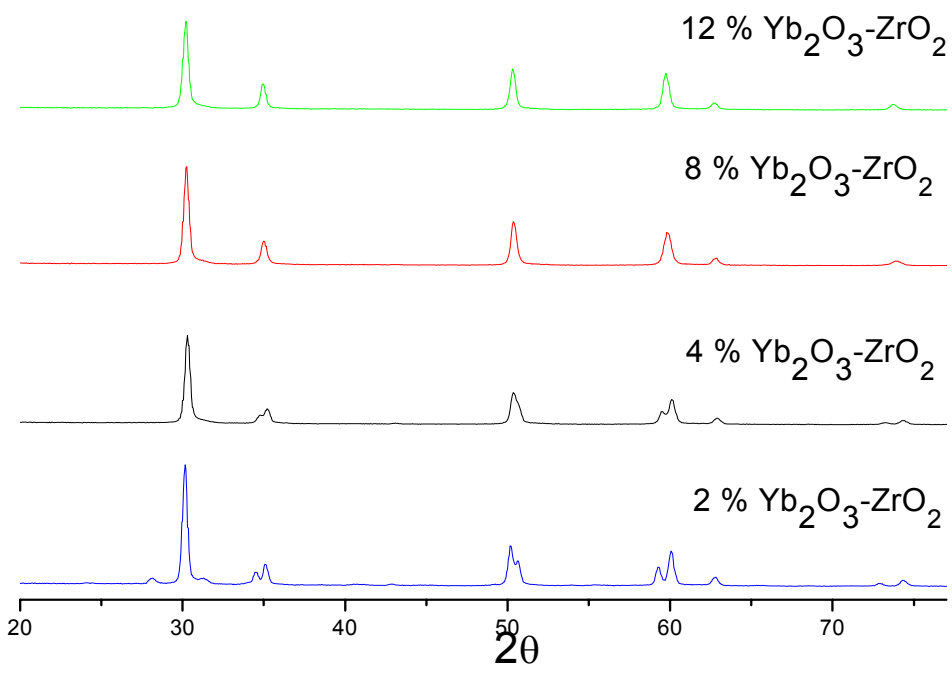

Fig. 5 The crystalline phase of the nanophosphor of ZrO2:Yb3+ is a mixture of phases monoclinic and tetragonal. For low concentrations of Yb (0.5%) the phase monoclinic predominates, while the phase tetragonal is the main component in high concentrations (2%). nevertheless, after 4% a transition is observed to the cubic phase, being this the only present when one has 12% Yb.

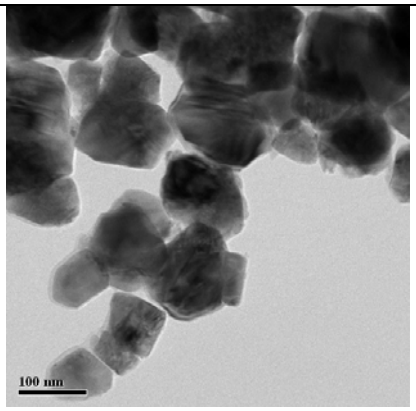

a) 0.5% Yb mainly monoclinic

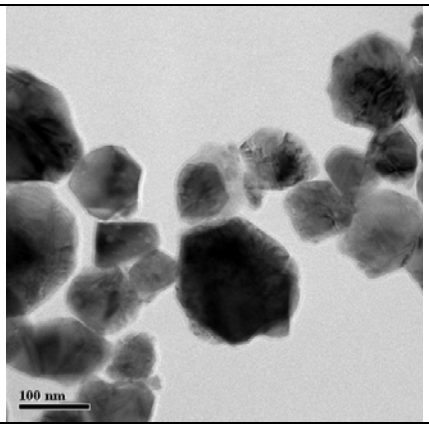

b) 2.0%Yb mainly tetragonal and little monoclinic

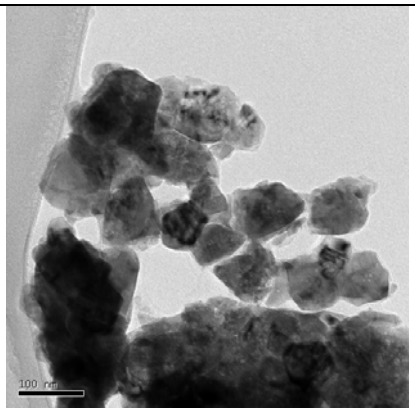

4.0% Yb pure cubic

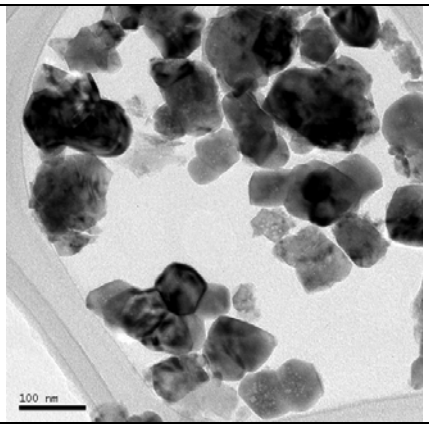

8.0% Yb pure cubic

Figure 6 crystallite size was confirmed with TEM

The absorption spectra of ZrO_2:Yb^{3+} nanophosphors, see fig. 7, present the characteristic broad absorption band of Yb^{3+} ion corresponding to $^2F_{7/2} \rightarrow {}^2F_{5/2}$ transition. Such band present characteristics peaks centered at 910, 942, 972 and 1002 nm and are in agreement with the results reported in different matrices. Notice the peak distribution change with the increment of Yb ions. That is due to the crystalline structure change given by the increment on Yb concentration and indicates the presence of different Yb sites within the ZrO_2. The spectra also show absorption bands centered at 310 nm and 260 nm characteristic of the monoclinic and tetragonal structure, respectively, reported previously [20]. The cubic structure (8%Yb) presents similar absorption bands than tetragonal. In addition, a strong broad absorption band centered at 453 nm was observed being stronger for higher Yb^{3+} concentration. We assume that such band corresponds to the cooperative absorption produced by the simultaneous excitation of two neighboring Yb ions. In the literature, it has been considered as a virtual state produced by the ionic interaction of Yb-Yb pairs. As mentioned earlier, few

papers have proposed that in some cases such pairs are bridged by an oxygen atom forming the system Yb-O-Yb [11,1]. In this case, the overlapping between the *Yb-4f* and the *O-2p* orbital enhance the interaction of active ion and then the cooperative absorption. Because this band is strong and corresponds to the self-convolution of the infrared (IR) band, see fig. 6, we believe it is the physical evidence of the existence of Yb^{3+} pairs bridged by an oxygen atom. Notice that no other detectable lines or bands corresponding to impurities of other rare earth ions or transition metals were observed in the visible region; in particular no Er^{3+} and Tm^{3+} impurities were observed.

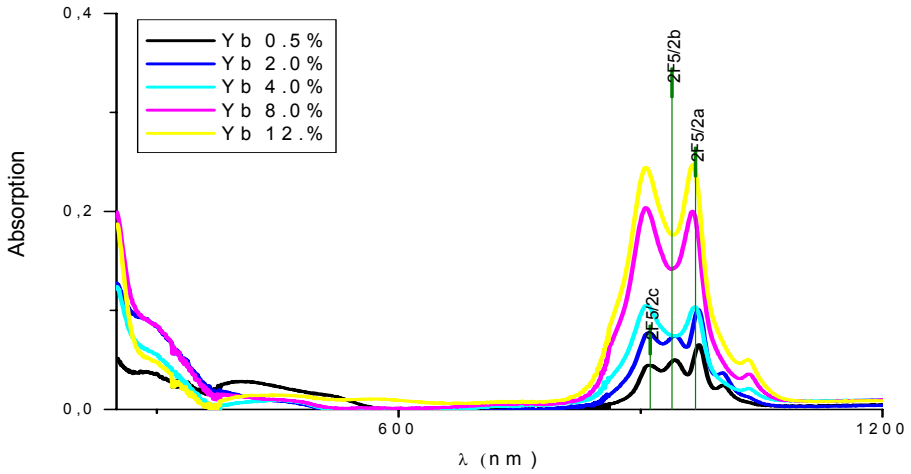

Fig. 7 The absorption spectra of ZrO_2:Yb^{3+} nanophosphors

The samples were pumped at 967 nm and the corresponding Yb^{3+} IR emission was collected with a PMT through a monochromator perpendicular to the pumping beam. Powder samples were deposited in a capillary tube hold by a special holder designed to maintain both same alignment condition and same quantity of active materials. The IR emission was in the expected range, see Fig. 8, but the Intensity trend of the spectra as the Yb_2O_3 concentration increases was not an increasing one. Fig. 8a clearly shows an initial increase from 0.5 up to 2.0% Yb3+ concentration, and then a reduction of luminescence from 2.0% up to 12% Yb concentration. That luminescence behavior is a typical example of luminescence concentration quenching. Curve a) in Figure 8b makes clearer the quenching behavior. That curve corresponds to the integrated intensity of the IR emission band. There we observe again that the 2% Yb concentration corresponds to the critical concentration for which the quenching becomes important.

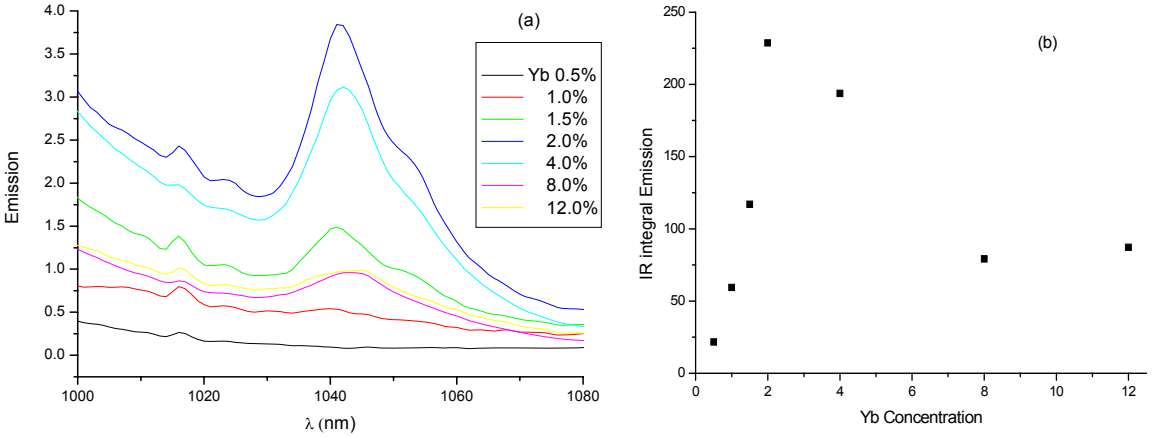

Fig. 8 a) IR emission and b) integrated intensity of the IR emission band

Now, the immediate question that arises is where does the quenched energy goes? And an interesting fact becomes as a possible response to such question: Besides the IR luminescence it is also observed strong blue-green emission. Figure 9a shows the visible emission band observed under 967nm pulsed pumping. Again it is observed a first increasing visible luminescence as Yb concentration increases up to 4%, and then a quenching of the visible luminescence becomes important up to 12% Yb^{3+}. Curve b) in figure 9b, shows the integrated intensity of the visible emission band. There it is clear, again, the quenching behavior of the visible luminescence. However the apparent critical concentration is, in this case, 4%Yb^{3+}.

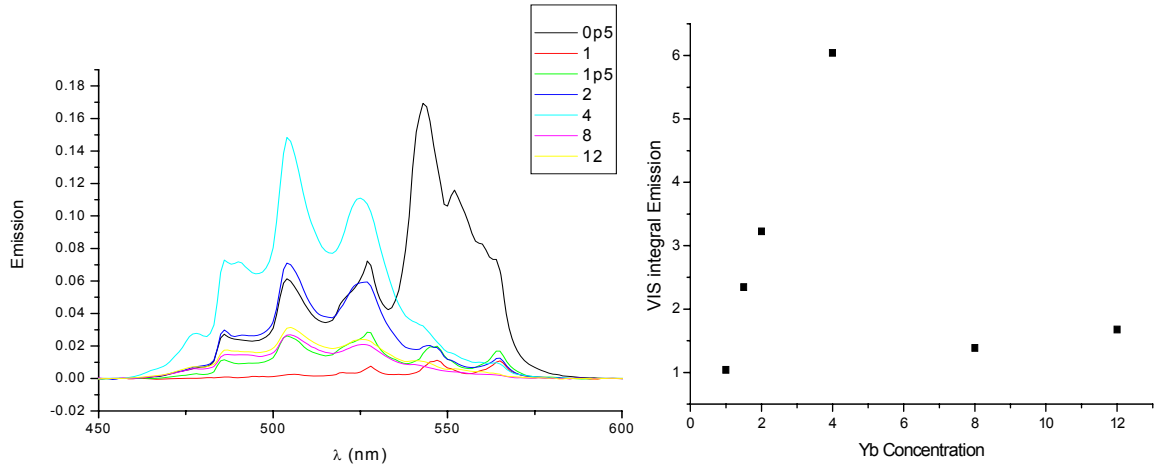

Fig. 9. a) VIS emission and b) integrated intensity of the VIS emission band

One could expect that if the reduction on IR emission was due to energy transfer to Yb^{3+} dimers, then as the concentration increases the quenching of IR should increase whit the consequent increase of visible emission from the dimers. In that sense one should expect that the addition of curves in figures 8b and 9b should result in at least a straight line whit positive slope. The slope being Yb^{3+} concentration dependent, since as the concentration increase the higher number of excitation photos absorbed by the sample that should be converted in Yb^{3+} emission whenever it is IR or visible. However, that is not the case. So the quenching trend has to be more complex, and it is clear that the sole evidence from the spectra is not enough to provide support for an adequate explanation of the phenomena. Besides, in spite of having taken the spectra under the same experimental conditions, there is always lack of calibration due to scattering and slight changes in alignment and sensibility of the detection system from sample to sample. So the best way to look at the possibility of quenching is be means of the measurement of the decay times of the excited level of Yb^{3+}. Figure 10, shows the decay time of the $^4F_{5/2}$ excited state of Yb^{3+} at 1041nm. For these measurements we used 25μm slits in the monochromator, and the pump was a CW diode laser at 967nm. The pump laser was modulated by a chopper at 100 Hhz. The PMT signal was collected by a 500 MHz Lecroy Oscilloscope. And the signal channel was set with a 50 Ohms impedance. From figure 10 it is clear that the quenching process starts even at the lowest concentration, since as the concentration increases the decay curve falls more rapidly. These tell us that the critical concentration is the smallest one we have, as far as we can observe. So the source of quenching has to be some centre that takes the energy away from the Yb^{3+} excited ions and is present for all concentrations. In addition that centers increases as the Yb^{3+} concentration increases. If we assume that the isolated Yb^{3+} emission has an intrinsic life time of about 1200 ms then its theoretical decay curve will be a straight line, see Fig. 10. By looking to the difference between the exponential decay of isolated ions (theoretical) and the experimental decays, we can conclude that the quenching process imprints a no exponential character to the experimental decays. That is a common characteristic of the decays of luminescence centers subject to non-radiative energy transfer process. The fact that the visible luminescence is present even at the lowest concentration and increases with increasing Yb concentration, gives support to presume that the quenching centers are the Yb

dimers [28, 29]. And the fact that its visible emission is quenched indicates that there is also interaction between these dimers and another center that could also be the very Yb^{3+} isolated ions.

In the fugure 11, we can see Quantum efficiency of the $^4F_{7/2}$ excited state of Yb^{3+} at 1041nm (We calculate the Quantum efficiency as lifetime of each concentration divided by lifetime of minor concentration samble). This figure shows a reduction of quantum efficiency as the Yb increase. That is the typical behaviour for luminescence concentration quenching.

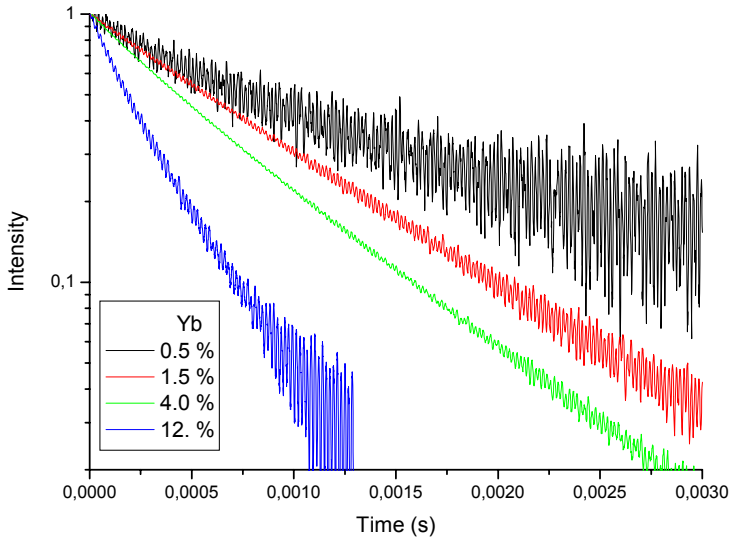

Fig. 10 Decay time of the $^4F_{7/2}$ excited state of Yb^{3+} at 1041nm

So far, we have shown that ZrO_2:Yb^{3+} is an interesting luminescent material where we have concentration quenching of the Yb^{3+} IR emission. In addition we observe the existence of strong visible emission which can be originated from Yb^{3+} dimers that act as the quenching centers for the Yb^{3+} IR emission. In the next chapters we will develop a teorethical model to approach the problem of the concentration quenching of a luminescent center as a consequence of the formation of pairs of the same center species.

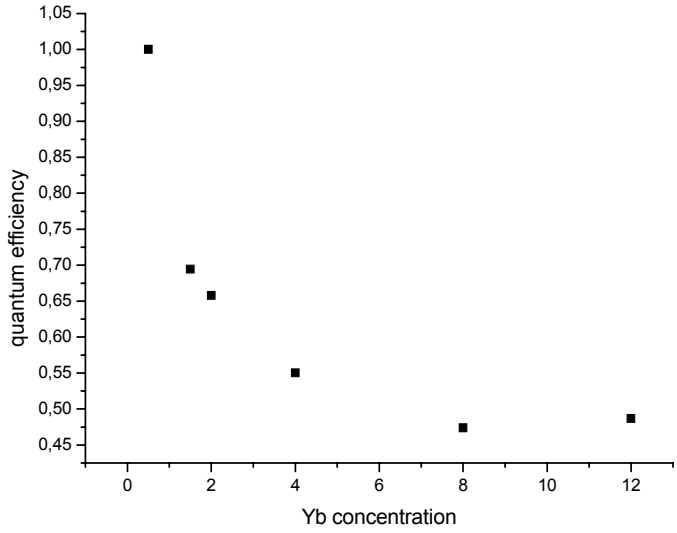

Fig. 11 Quantum efficiency of the $^4F_{7/2}$ excited state of Yb^{3+} at 1041nm

References

1. Takugo Ishii, First-principles calculations for the cooperative transitions of Yb^{3+} dimer clusters in $Y_3A_{l5}O_{12}$ and Y_2O_3 crystals, THE JOURNAL OF CHEMICAL PHYSICS 122, (2005)
2. J. Garcia Solé, *Optical Spectroscopy of Inorganic Solids,* ed. Wiley (2005)
3. Michel Digonnet, *Rare earth doped fiber lasers and amplifiers,* Ed Marcel Dekker (2001)
4. R. Paschotta, J. Nilsson, P.R. Barber, J.E. Caplen, A.C. Tropper, D. C. Hanna. *Lifetime quenching in Yb-doped fibers*. Opt. Commun. 136:375-378. 1997
5. V.P. Gapontsev. In: *Phosphate Laser Glasses*. Science, Moscow, 174-386, 1980.
6. E. Nakazawa and S. Shionoya, Phys. Rev. Lett. 25, 1710 (1970).
7. E. De la Rosa, P. Salas, L. A. Diaz-Torres, *Strong Visible Cooperative Up-Conversion Emission in* $ZrO_2:Yb^{3+}$ *nanocrystals.* Journal Nonoscience and Nanotechonlogy Vol. 5,1480-1486, 2005
8. Ph. Goldner, F. Pelle, D. Meichenin, and F. Auzel, J. Lumin. 71, 137 (1997).
9. B. Z. Malkin, A. M. Leushin, A. I. Iskhakova, J. Heber, M. Altwein, K. Moller, I. I.

Fazlizhanov, and V. A. Ulanov, Phys. Rev. B 62, 7063 (2000).
10. M. P. Hehlen and H. U. Gudel, J. Chem. Phys. 98, 1768 (1993).
11. H. J. Schugar, E. I. Solomon, W. L. Cleveland, and L. Goodman, J. Am. Chem. Soc. 97, 6442 (1975).
12. W. Chen, J.Z. Zhang and A.G. Joly, J. Nanosci. Nanotech. 4, (2004) 919-947
13. P.K. Sharma, M.H. Jilavi, R. Nass and H. Schmidt, J. Lumin. 82, (1999) 187-193
14. Y.L. Soo, S.W. Huang, Z.H. Ming, Y.H. Kao, G.C. Smith, E. Goldburt, R. Hodel, B. Kulkarni, J.V.D. Veliadis and R.N. Bhargava, J. Appl. Phys. 83, (1998) 5404-5409
15. R.S. Meltzer, W.M. Yen, H. Zheng, S.P. Feofilov, M.J. Dejneka, B.M. Tissue and H.B. Yuan, Phy. Rev. B, (2001) 100201
16. C.H. Lu, H.C. Hong and R. Jagannathan, J. Mat. Chem. 12, (2002) pp 2525-2530.
17. E. De la Rosa-Cruz, L. A. Díaz-Torres, P. Salas, R. A. Rodríguez, G. A. Kumar, M. A. Meneses, J. F. Mosiño, J. M. Hernández and O. Barbosa-García, J. Appl. Phys., 94, (2003) pp 3509-3515.
18. J. Silver, M.I. Martinez-Rubio, T.G. Ireland, G.R. Fern and R. Withnall, J. Phys. Chem. B, 105, (2001) pp 948-953.
19. E. De la Rosa-Cruz, L.A. Díaz-Torres, R.A. Rodríguez-Rojas, M.A. Meneses-Nava, O. Barbosa-Garcia and P. Salas, Appl. Phys. Lett., 83**,** (2003) pp 4903-4905.
20. J.C. Boyer, F. Vetrone, J.A. Capobianco, A. Speghini and M. Bettinelli, Chem. Phys. Lett. 390, (2004) 403-407
21. J. Dong, M. Bass, Y. Mao, P. Deng and F. Gan, J. Opt. Soc. Am. B, 20, (2003) 1975-1979
22. S.M. Redmond, S.C. Rand and S.L. Oliveira, Appl. Phys. Lett. 85, (2004) pp 5517-5519
23. M.P. Hehlen, A. kuditcher, S.C. Rand and S.R. Luthi, Phys. Rev. Lett. 82, (1999) 3050-3053
24. M. Malinowski, M. Kaczkan, R. Piramidowicz, Z. Frukacz and J. Sarnecki, J. Lumin., 94-95, (2001) pp 29-33.
25. M.A. Noginov, G.B. Loutts, C.S. Steward, B.D. Lucas, D. Fider, V. Peters, E. Mix and G. Hiber, J. Lumin. 96, (2002) pp 129-140.
26. Patra, S. Saha, M. Alencar, N. Rakov, G. Maciel; Chem. Phys. Lett. 407, 477(2005).

27. W. Córdova-Martínez, E. De la Rosa-Cruz, L.A. Díaz-Torres, P. Salas, A. Montoya, M. Avendaño, R.A. Rodríguez and O. Barbosa-García; Opt. Mat., 20, (2002) 263-271
28. P. Salas, E. De la Rosa, R.A. Rodríguez, D. Solis, C. Angeles-Chevez. to be published
29. P. Salas, C. Angeles-Chávez, J.A. Montoya, E. De la Rosa, L.A. Díaz-Torres, H. Desirena, A. Martínez, M.A. Romero-Romo and J. Morales, Opt. Mater. 27, (2005) pp 1295-1300
30. Steven M. Massey, Jason B. McKay, Diode-pumped Nd:YAG and Nd:glass spinning-disk lasers, Vol. 22, No. 5/May 2005/J. Opt. Soc. Am. B
31. Alexander V. Kir'yanov, Yuri O. Barmenkov,Cooperative luminescence and absorption in Ytterbium-doped silica fibers and the fiber nonlinear transmission coefficient at λ = 980 nm with a regard to the Ytterbium ion-pairs' effect. Vol. 14, Iss. 9 -May 2006. Optics Express.
32. Dexter, Phys. Rev. **126**, 1962.
33. L.A. Diaz-Torres, E. De la Rosa, *Enhanced cooperative absorption and upconvertion in Yb^{3+} doped YAG nanophosphors*, Optical Materials 27 (2005) 1305-1310.

Chapter 2:

Non radiative Energy transfer in crystals.

1. Introduction

The work of this thesis is enclosed in the extensive research area of development and optimization of luminescent materials, specifically of solid-state luminescent phosphors doped with rare-earth ions. Given that the doping ions are responsible for the luminescence, one could think that higher doping concentrations would result in higher laser output power. However, as we shown at the preceding chapter, reality is quite different, optimum concentration values lay around 2 %mol doping concentration. At least for Yb3+ doped ZrO_2. In fact, it is known that in general the optimun doping concentration of Rare earths in solid state host is around 1 %at [1,2,3].

In general, the doping ions in crystal phosphors interact with both, the host lattice and other doping ions. When some resonant transitions exist between the interacting doping ions, some non-radiative energy transfer processes create additional relaxation channels that diminish the quantum efficiency of the phosphor. That is a reduction of the life time becomes evident. Non-radiative energy transfer phenomena have been known in solid phosphors and solutions long before lasers were invented and their study is still an active research field [1-6]. In the particular field of laser materials, not all the effects of non-radiative energy transfer are negative. While some studies evaluate detrimental effects of energy transfer on laser performance [7], some others evaluate benefits from such processes in alternative to optical pumping mechanisms for co-doped solid state lasers, either with flash lamps or diode laser arrays [8]. The study of non-radiative energy transfer processes can also help to find more convenient dopant concentrations for luminescent materials [6].

The theoretical studies on non-radiative energy transfer processes also have a long history. Since the 1920's, different research groups have been modelling the non-radiative energy transfer processes in different materials [9-10]. However, the theoretical models available nowadays do not fully describe and characterize the

luminescent properties of luminescent materials. Thus, a common procedure to obtain better phosphors has been the time consuming "trial and error" method. A better understanding of the microscopic nature of non-radiative energy transfer processes is needed for the development of new luminescent materials since it will allow the prediction of optimum parameters for preparation and use of single doped and co-doped luminescent materials.

The analysis of non-radiative energy transfer processes made in this thesis is based on a numerical solution for the General Energy Transfer Master Equations (GETME) in crystalline co-doped materials [14]. The GETME are up to now only applicable for systems in which the active ions have only two energy levels and the transition energies are resonant, or phonon assisted resonant. In this chapter the non resonant case will be discussed as well as the resulting nonlinearity of this consideration. Besides we have considered more energy levels of the involved ions. This last consideration is due to the fact that for considering unconversion processes a more realistic model have to take in to acount the intermediate level that is promoted to the upconversion level. Thus we edn with a more general nonlinear model for energy transfer process in crystals that can take into account the upconvesrsion processes at the simplest lcomplexity. It is our goal for the next chapther to apply such model in oreder to explain the quenching of the IR fluorescence of Yb^{3+} in ZrO_2, already presented in the previous chapter.

2. Fundamentals of non-radiative energy transfer.

The modelling of non-radiative energy transfer phenomena is not an easy task since for any given host material a variety of processes may occur between the doping ions (i.e. direct energy transfer, energy migration, energy back transfer, energy up-conversion and energy trapping). Each of these processes can be driven by more than one microscopic electronic interaction among dopants. The effects of non-radiative energy transfer processes are evident on the luminescence transients (luminescence decay) recorded from doped samples. For non-interacting ions, the temporal behavior of the luminescence follows an exponential decay but, when some energy transfer processes are present, the dopant macroscopic emission becomes non-exponential. In fact, recent measurements have recorded complex temporal transients of the

luminescence for certain laser materials, which indicates that interactions among dopants can be quite complex indeed [10-13].

The microscopic origin for non-radiative energy transfer processes can be visualized as an interaction between an excited ion, the donor D, and another not excited ion, the acceptor A, with an absorption transition resonant with the de-excitation of the first one. If $|d\rangle$ and $|d'\rangle$ correspond to eigenfunctions of the lower and upper states of the transition in the donor ion while $|a\rangle$ and $|a'\rangle$ are the corresponding eigenfunctions for the acceptor ion, then for an initial state where only the donor ion is excited the corresponding eigenstate of the combined system of donor-acceptor will be $|d'a\rangle$. After the non-radiative energy transference from D to A takes place, the eigenstate of the combined system will be $|da'\rangle$. The probability for the transition $|d'a\rangle \rightarrow |da'\rangle$ to occur represents the transfer rate of excitation energy from ion D to ion A, $W(D \rightarrow A)$, which is given by [12, 13,23]

$$W(D \rightarrow A) = \left(\frac{4\pi^2}{h}\right) \langle d'a | H_{DA} | da' \rangle^2 \int g_D^{EMISSION}(E)\, g_A^{ABSORTION}(E)\, dE \qquad (1)$$

where h is the Planck's constant, H_{DA} is the Hamiltonian of the interaction between donor and acceptor, $g_D^{EMISSION}(E)$ and $g_A^{ABSORTION}(E)$ are the normalized line shapes of the transitions $|d\rangle \rightarrow |d'\rangle$ and $|a\rangle \rightarrow |a'\rangle$ respectively.

The electronic interactions to consider, between ion D and ion A, are the Coulomb interaction and the exchange interaction. The Hamiltonian for the Coulomb interaction for electrons in the two ions is given by,

$$H_{DA} = q_e^2 \left| \vec{R}_{DA} + \vec{r}_d - \vec{r}_a \right|^{-1} \qquad (2)$$

where $\vec{R}_{DA}$ is the vector distance from ion D to ion A, $\vec{r}_d$ and $\vec{r}_a$ are the position vectors of the electrons around each ion, and q_e is the fundamental electronic charge.

2.1 Exchange interaction.

The Exchange interaction is due to the overlap of the antisymmetric wave functions of the D and A ions, and therefore it is an interaction of very short reach. This interaction decays exponentially with the distance $\left(R_{X_iY_j}\right.$ with $\left.X,Y=D,A\right)$ between ions. We can write the Exchange interaction as [14]

$$W_{X_iY_j}^{Exchange}\left(R_{X_iY_j}\right)=\frac{1}{\tau_{X_o}}\exp\left(\frac{2R_o^{XY}}{L^{XY}}\right)\exp\left(-\frac{2R_{X_iY_j}}{L^{XY}}\right) \tag{3}$$

The free parameters for the exchange interaction are R_o^{XY}, τ_{X_o} and L^{XY}, the critical transfer distance, the free lifetime of the ion X and the effective Bohr's radius, respectively.

We can interpret R_o^{XY} as the distance for which the transfer rate is equal to the free X-ion lifetime, that is

$$W_{X_iY_j}^{Exchange}\left(R_o^{XY}\right)=\frac{1}{\tau_{X_o}}$$

2.2 Electrostatic Interaction

The electrostatic interaction is a result of the interaction of the electric fields of the ions inside the crystal host; it is considered that it is an interaction of long reach. The electrostatic interaction can be decomposed in a multi polar expansion, where the most important terms are dipole-dipole, dipole-quadrupole and quadupole-quadrupole. The transfer rate by the electrostatic interaction among the D and A ions can be written as [14]

$$W_{D_iA_j}^{elec}\left(R_{D_iA_j}\right)=\frac{1}{\tau_{D_o}}\left[\left(\frac{R_{06}}{R_{D_iA_j}}\right)^6+\left(\frac{R_{08}}{R_{D_iA_j}}\right)^8+\left(\frac{R_{010}}{R_{D_iA_j}}\right)^{10}\right] \tag{4}$$

R_{0S} defines the critical distance of transfer and the values of S = 6,8,10 define the type of interaction: dipole-dipole, dipole-quadrupole and quadupole-quadrupole, respectively.

The interactions above described are responsible of the interionic processes that involve the direct transfer of excitation energy between two ions without the absorption or emission of phonons and that is why, in general, such processes are known as resonant non-radiative energy transfer.

2.3 Interionic Processes

The main different interionic processes arising as a consequence of energy transfer process appear in the literature as (see fig. 2.1): Cross-Relaxation, Upconversion and Energy-Migration.

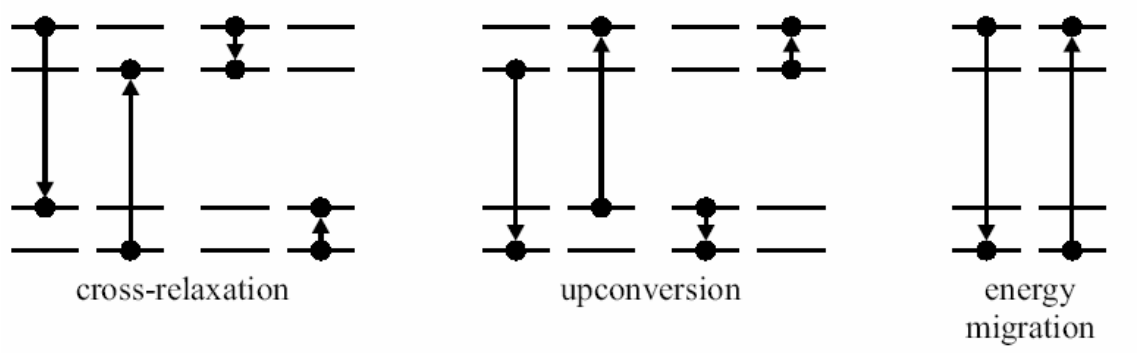

Fig 1 Interionic processes

Cross-Relaxation

Cross-relaxation is the full or partial transfer of excitation energy to an acceptor in a lower level. This process can be very efficient, if the energy differences in the participating donor and acceptor levels are resonant or the energy needed to excite the acceptor is slightly smaller than the energy provided by the donor. Crossrelaxation is often used to sensitize ions with small absorption cross section by codoping with ions with strong absorption, like ytterbium, to achieve a more efficient excitation.

Upconversion

Upconversion is similar to cross relaxation except that the acceptor is initially in an excited state. The resulting excitation energy of the acceptor is higher than the original excitation energy of the donor. This process allows the realization of lasers with a shorter emission- than pump-wavelength [15].

Energy-Migration

Energy migration is the resonant energy transfer between two ions of the same type. This process allows the excitation energy to quickly spread out and therefore raises the probability of the other energy transfer processes. Energy migration is described by several models depending on the ratio of transfer rates between two donors C_{DD} and between donor and acceptor C_{DA}. Right after the excitation a fast migration of the excitation energy between donors occurs [16]. After this first, fast migration to neighboring ions, the further spreading of energy can be either described by the diffusion-model in the case that C_{DD} is much smaller than C_{DA} [17] or the hopping-model for C_{DD} larger than C_{DA} [18].

Due to the strong dependence of the energy transfer transition probabilities on the distance between donor and acceptor, the energy transfer processes become most important at high doping levels, when the distances among active centers are reduced as a result of the increasing concentration of active centers. This can be very useful if energy transfer is desired as in sensitized systems or can be harmful if the excitation energy is transferred away from the active ion to unwanted impurities. In the case of highly doped ytterbium systems, energy transfer to such impurities can cause a nearly complete quenching of the excitation energy and therefore make laser operation impossible. The energy quenching of $Yb_3Al_5O_{12}$ and $Yb:RE_2O_3$ has been investigated in the works of V. Müller and A. Bolz [19,20]. And we have shown its effects on ZrO2 in the previous chapter.

3. Rate Equation Analysis for Non Radiative Energy transfer: The General Energy Transfer Master Equations (GETME).

Experimental measurements of spectral properties such as the fluorescence intensities and fluorescence lifetimes as function of variables such as temperature, active ion concentration, and lifetime can be used to obtain independent estimates of these same parameters. The comparison between theoretical and experimental estimates is used to answer these questions about the properties of energy transfer. The most common procedure has been to study the "concentration quenching" of fluorescence intensity. That is, one observes the variations on intensity spectra as the dopant concentration changes. The major problem with this technique requires accurate knowledge of the concentration on active ions in a series of samples and a calibrated reference luminescent phosphor for which one has a very accurate knwoledge of the dopant concentration. That is generally is not available. Measurement of the time evolution of fluorescence is easiest and if enough information is know about the material, it is possible to obtain theoretical estimates of all of the relevant parameters from the theoretical models described in the book Physics of Solids-State Laser Materials of Powell [14].

The most general expression for the evolution of energy away from an initially exited ion is [14]

$$\frac{dP_i(t)}{dt} = -\left(\beta + \sum_j W_{ij} + \sum_{n\neq i} w_{in}\right) P_i(t) + \sum_j W_{ji} P_j(t) + \sum_{n\neq i} w_{ni} P_n(t) \tag{5}$$

Where $P_i(t)$ is the probability to finding the excitation at the ith sensitizer (Donor) ion at time t, beta is the intrinsic fluorescence decay rate of sensitizer ions, W_{ij} is the energy transfer rate from sensitizer i to activator (Acceptor) j and W_{ji} is the transfer in the opposite direction (back transfer), w_{in} describes the energy migration among sensitizer ions before fluorescence or transfer to an activation ions occurs. This equation must be solved and the results are related to experimental observables such as the fluorescence intensity. This requires performing a configuration average after the distribution of all possible ion-ion interaction and the inclusion of the initial conditions. Although

attempts have been made to develop a general solution to this equation, this is a difficult task since a double configuration average is required to account for both spatial disorder (random location of ions) and spectral disorder (variation of transition energies from site to site as reflected in inhomogeneous broadening of spectral lines). Knowing the details of these distributions is critical in understanding the physics of energy transfer in a particular case. For example, the time dependence of energy transfer is significantly different if the sensitizer and activator ions are located in pairs, all having the same separation, randomly separated pairs, or distributed with all of sensitizer on one side of the sample and all activators on the other side. However, for most practical case with solid-state phosphors, it is sufficient to assume a random spatial distribution of activator with the uniformly exited sensitizers either having a similar random distribution or, for host-sensitizer case, being distributed in a known lattice configurations. Also, in general the spectral distribution is most important al low temperature and can be ignored at room temperature where phonons are available to bring transitions of neighboring ions in to phonon assisted resonance with each other.

So far, the Transfer Master Equations, Eqs. 5, are up to now only applicable for systems in which the ions have only two energy levels and their energy levels are in a resonance condition, phonon assisted or not. In the following sections the non resonant case will be discussed as well as the resulting nonlinearity of this consideration. Besides we have considered more energy levels of the involved ions.

In order to relate the microscopic transfer rates, Eqs. 4 and 3, to observable quantities an average over a macroscopic sample containing many donor and acceptor ions must be performed. ln a sample with N_D donors and N_A acceptors we have to deal with an ensemble of ions where every donor has a particular environment of N_A acceptors at different distances. There are two measurable quantities that provide some information about the energy transfer from donors to acceptors. They are the time development of the donor's luminescence after pulsed excitation $\phi(t)$, and the relative quantum yield, which is the ratio between the time integral of $\phi(t)$ and the radiative lifetime that the transition would have if acceptors were absent.

To obtain an expression for $\phi(t)$, we first consider the probability for the i-th donor to be excited at time t as $P_{D_i^1}(t)$ and similarly for the j-th acceptor we have $P_{A_j^1}(t)$. The dynamics of these probabilities, for a co-doped sample with N_D donors and N_A acceptors, can be expressed by the coupled differential equations:

$$\frac{dP_{D_i^1}}{dt} = -\left(\frac{1}{\tau_{Do}} + \sum_{k=1}^{N_A} W_{D_i^1}^{A_k^1} + \sum_{k=1}^{N_D} W_{D_i^1}^{D_k^1}\right) P_{D_i} + \sum_{k=1}^{N_A} W_{A_k^1}^{D_i^1} P_{A_k^1} + \sum_{k=1}^{N_D} W_{D_k^1}^{D_i^1} P_{D_k^1} \tag{6}$$

$$\frac{dP_{A_j^1}}{dt} = -\left(\frac{1}{\tau_{Ao}} + \sum_{k=1}^{N_A} W_{A_j^1}^{A_k^1} + \sum_{k=1}^{N_D} W_{A_j^1}^{D_k^1}\right) P_{A_j} + \sum_{k=1}^{N_A} W_{A_k^1}^{A_j^1} P_{A_k^1} + \sum_{k=1}^{N_A} W_{D_k^1}^{A_j} P_{D_k^1} \tag{7}$$

These equations are obtained by following the master equations proposed by Powell [14], and extending the model to include the acceptor subsystem [21,23].

On the equations 6 and 7, τ_{D_O} and τ_{A_O} are the radiative lifetimes of donor and acceptor ions respectively. These lifetimes are measured under conditions where energy transfer process can be neglected. The transfer rates involved in both equations correspond to the different energy transfer processes that may occur in a given sample for donor-acceptor interactions and donor-donor interactions, as well as acceptor-aceptor interactions. $W_{D_i^1}^{A_k^1}$ corresponds to the non-radiative energy transfer rate from D_i^1 to A_k^1 and defines the process known as direct energy transfer (DET) from donors to acceptors.- $W_{D_i^1}^{D_k^1}$ is the non-radiative energy transfer rate from D_i^1 to D_k^1 and together with $W_{D_k^1}^{D_i^1}$ define the process known as energy migration among donors (EMAD). $W_{A_j^1}^{D_k^1}$ is the non-radiative energy transfer rate from A_j^1 to D_k^1 and defines the energy back transfer (EBT) process from acceptors to donors. $W_{A_j^1}^{A_k^1}$, is the non-radiative energy transfer rate from A_k^1 to A_j^1 and together with $W_{A_k^1}^{A_j^1}$ define the process known as energy migration among acceptors (EMAA). Each of these energy transfer rates can be expressed in terms of the microscopic interaction parameters given by equations 4 or 3 or a sum of them. Here, we call equations 6 and 7 as the General Energy Transfer Master Equations (GETME). As noted before, the microscopic interaction parameters

can be obtained either from a microscopic approach through transition probability calculations or, from fitting the experimental measurements of the fluorescence decay of dopants in macroscopic samples. The solution for equations 6 and 7 is:

$$P = P_o e^{Kt} \tag{8}$$

where

$$P = \begin{bmatrix} P_{D_1}(t) \\ \vdots \\ P_{D_{N_D}}(t) \\ P_{A_1}(t) \\ \vdots \\ P_{A_{N_A}}(t) \end{bmatrix} \tag{9}$$

$$P_o = \begin{bmatrix} 1 \\ \vdots \\ 1 \\ 0 \\ \vdots \\ 0 \end{bmatrix} = \begin{bmatrix} P_{D_1}(0) \\ \vdots \\ P_{D_{N_D}}(0) \\ P_{A_1}(0) \\ \vdots \\ P_{A_{N_A}}(0) \end{bmatrix} \tag{10}$$

and

$$K = \begin{bmatrix} -T_{D_1}^{D_1} & \cdots & W_{D_{N_D}}^{D_1} & W_{A_1}^{D_1} & \cdots & W_{A_{N_A}}^{D_1} \\ \vdots & \ddots & \vdots & \vdots & \ddots & \vdots \\ W_{D_1}^{D_{N_D}} & \cdots & -T_{D_{N_D}}^{D_{N_D}} & W_{A_1}^{D_{N_D}} & \cdots & W_{A_{N_A}}^{D_{N_D}} \\ W_{D_1}^{A_1} & \cdots & W_{D_{N_D}}^{A_1} & -T_{A_1}^{A_1} & \cdots & W_{A_{N_A}}^{A_{N_A}} \\ \vdots & \ddots & \vdots & \vdots & \ddots & \vdots \\ W_{D_1}^{A_{N_A}} & \cdots & W_{D_{N_D}}^{A_{N_A}} & W_{A_1}^{A_{N_A}} & \cdots & -T_{A_{N_A}}^{A_{N_A}} \end{bmatrix} \tag{11}$$

Where

$$T_{D_i}^{D_i} = \frac{1}{\tau_{Do}} + \sum_{k=1}^{N_A} W_{D_i^1}^{A_k^1} + \sum_{k=1}^{N_D} W_{D_i^1}^{D_k^1} \quad , i = 1..N_D \tag{12}$$

$$T_{A_j}^{A_j} = \frac{1}{\tau_{Ao}} + \sum_{k=1}^{N_A} W_{A_j^1}^{A_k^1} + \sum_{k=1}^{N_D} W_{A_j^1}^{D_k^1} \quad , j = 1..N_A \tag{13}$$

To compare the predictions from the quantum mechanical calculations with the experimental results or to obtain the values for the microscopic interaction parameters from experimental measurements, an average of $P(t)$ over a macroscopic sample has to be performed. It is worth to notice that one of the main differences, among the models developed up to now, is the way in which such macroscopic average is obtained. A good review of the previous models can be found in [21,22,23].

So, once the individual excitation probabilities are known for each dopant in the crystal sample, we can determine that mean excitation probability that the donor ensemble remains excited at time t. The mean excitation probability value gives the average number of donors in the excited state and therefore is proportional to the normalized donor fluorescence from the crystalline sample,

$$\left[P_D(t)\right]_k = \frac{\sum_{i=1}^{N_D}\left[P_{D_i}(t)\right]_k}{\sum_{i=1}^{N_A}\left[P_{A_i}(0)\right]_k + \sum_{i=1}^{N_D}\left[P_{D_i}(0)\right]_k} \tag{14}$$

If this probability is averaged over a large number of randomly generated crystal samples, k, the resulting average converges to the macroscopic donor fluorescence decay $\phi_D(t)$,

$$\phi_D(t) = \frac{1}{N_m}\sum_{k=1}^{N_m}\left[P_D(t)\right]_k \tag{14a}$$

An analogous argument is valid for the acceptor fluorescence

$$\phi_A(t) = \frac{1}{N_m}\sum_{k=1}^{N_m}\left[P_A(t)\right]_k \tag{14b}$$

Thus, these last 8 Eqs. Allow us to theoretically predict the decay dynamics of the active ions (D and A) whiting a crystalline sample. Details of the numerical

implementacion are given in Apendix A. This prediction can be compared against the experimental ones in order to find the microscopic interaction parameters that drive the energy transfer processes responsible of the experimental decat trend.

As has been mentioned above, when dealing with energy transfer prcesses in most of the current models it is considered that the energy transfer is driven by a weak interaction between D and A ions, and that the transition energy gaps of the individual ions are shifted by amounts smaller that the widths of the levels. That is, the process is almost resonant, or as sometimes is known in the literature, it is a phonon assisted non radiative energy transfer process. Next, we show that when taking in to account the population of the ions in the ground state and the off-resonance reality, the master equations that govern the dynamics of luminescence are in fact non linear equations, that in turn reduce to the GETME under very specific conditions. So, in order to continue in such direction first we will review again what resonance means.

Phonon-Assisted energy transfer

To allow energy transfer, some interaction mechanism between the excited donor D and de acceptor A is needed. In fact, the probability of energy transfer from the donor centers to the acceptor centers is given by Eq. 1:

$$W(D \to A) = \left(\frac{4\pi^2}{h} \right) \langle d'a | H_{DA} | da' \rangle^2 \int g_D^{EMISSION}(E)\, g_A^{ABSORTION}(E)\, dE \qquad (1)$$

The integral represents the overlap between the donor emission line-shape, $g_D^{EMISSION}$, and the acceptor absorption line-shape, $g_A^{ABSORTION}(E)$; and works as a normalization factor of the transition matrix element. Such normalization constant has a maximum when D and A are centers that posses coincident energy level gaps. That is, they fulfill a condition known as “having resonant gap energies”. Such condition can be fulfilled only when both ions are of the same species. Neverteless, in the literature, when it is assumed that such condition is fulfilled the energy transfer process is known as “resonant energy transfer”, even if the involved ions are different species.

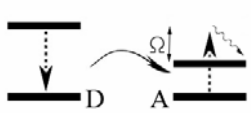

Fig. 2 Phonon-assisted energy transfer.

However, when D and A are different species, is usual to find a energy mismatch between the transitions of the donor and acceptor ions (see Fig 2). In this case, the energy transfer process needs to be assisted by lattice phonons of appropriate energy, $\Omega = \pm h\omega$, and this is usually called "phonon-assisted energy transfer". In these energy transfer processes, electron-phonon coupling must be also taken into account, together with the interaction mechanism responsible for the transfer.

4. Energy transfer among two energy level ions Revisited: The Non Linear General Energy Transfer Master Equations (NLGETME)

Let us consider at the moment that the ions in the crystal host are of the type D and A, and that both species have only two energy levels. The D and A ions are distributed in the possible places of the crystalline lattice and they are separated by a distance $R_{D_iA_j}$. $R_{D_iA_j}$ is a discreet aleatory variable that depends on the dopants concentration as well as the crystalline phase of the material.

Let us consider that the i-th donor is excited at t=0 and it can transfer its energy to another ion inside the crystal. It is convenient to define some variables: $P_{D_i}^1(t)$ as the individual probability of the i-th donor remains excited at the time t, $P_{A_j}^1(t)$ as is the individual probability of the j-th acceptor to remain excited at the time t, $P_{D_i}^0(t)$ as the individual probability of the i-th donor being in its ground state at the time t, $P_{A_j}^0(t)$ as the individual probability of the that j-th acceptor is in the ground state at the time t. These probabilities should fulfill that

$$P_{A_j}^1(t) + P_{A_j}^0(t) = 1 \tag{15}$$

$$P_{D_j}^1(t) + P_{D_j}^0(t) = 1 \tag{16}$$

Now, once the i-th donor is excited it has the following possibilities to give up its energy:

1.- The i-th donor can lose energy by a radiative transition (see fig. 3) with a rate

$$\frac{1}{\tau_{D_o}} \tag{17}$$

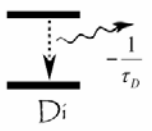

Figure 3 The donor i-th can lose energy by a radiative transition emitting a photon

Then the change of individual probability of the i-th donor is the product of the radiative relaxation rate times the probability that the ion is excited $P_{D_i}^1(t)$, that is to say

$$\frac{1}{\tau_{D_o}} P_{D_i}^1(t) \tag{18}$$

2.- The i-th donor can non radiatively transfer its energy to a j-th acceptor at a distance $R_{D_iA_j}$ with a transfer rate,see fig 4,

$$W_{D_i^1}^{A_j^1}\left(R_{D_iA_j}\right) \tag{19}$$

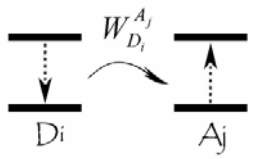

Figure 4 Direct Transfer (DT) donor→acceptor

The notation used for the energy transfer rate is

$$W_Y^X\left(\mathrm{R_{DA}} = \text{distance between X and Y ions}\right) \tag{20}$$

where X it indicates the ion that receives the excitation energy after the transfer as well as its ending state, and Y indicates the initially excited ion that gives up its excitation energy during the transfer process. Thus the decrement of the individual probability of the i-th donor is the product of the transfer rate by the probability that the ion D_i is excited $P_{D_i}^1(t)$ and that the ion A_j is in the ground state $P_{A_j}^0(t)$, that is to say

$$W_{D_i^1}^{A_j^1}\left(R_{D_iA_j}\right)P_{D_i}^1(t)P_{A_j}^0(t) \tag{21}$$

This process is known as Direct Transfer (DT) $donor \rightarrow acceptor$

3.- The i-th donor can give its energy to a j-th donor that is at a distance $R_{D_iD_j}$ with a transfer rate (to see fig 5)

$$W_{D_i^1}^{D_j^1}\left(R_{D_iD_j}\right) \tag{22}$$

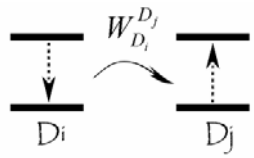

Figure 5 Migration between Donors (MD) donor→donor

Then the decrement of the individual probability of the i-th donor is the product of the transfer rate for the probability that the ion D_i is excited $P_{D_i}^1(t)$ and the ion D_j is in the ground state $P_{D_j}^0(t)$, that is to say

$$W_{D_i^1}^{D_j^1}\left(R_{D_iD_j}\right)P_{D_i}^1(t)P_{D_j}^0(t) \tag{23}$$

This process is known as Migration between Donors (MD) $donor \rightarrow donor$

Now, besides the above described processes, the ion D_i also can receive energy in the following ways:

4.- The ion D_i can receive energy of an ion A_j that is excited at a distance $R_{D_iA_j}$ with a transfer rate (to see fig 6)

$$W_{A_j^1}^{D_i^1}\left(R_{D_iA_j}\right) \tag{24}$$

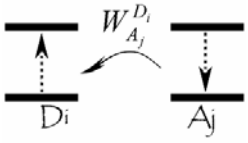

Figure 6 Acceptor Back Transfer donor←acceptor

Since A_j has a probability $P_{A_j}^1(t)$ of being excited, then the probability that D_i remains excited will be increased for

$$W_{A_j^1}^{D_i^1}\left(R_{D_iA_j}\right)P_{D_i}^0(t)P_{A_j}^1(t) \tag{25}$$

This process is known as Acceptor Back Transfer (ABT) *donor* ← *acceptor*

5.- The ion D_i can receive energy of an ion D_j that is excited at a distance $R_{D_iD_j}$ with a transfer rate (to see fig 7)

$$W_{D_j^1}^{D_i^1}\left(R_{D_iD_j}\right) \tag{26}$$

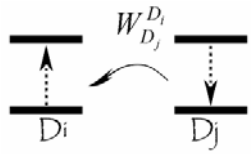

Figure 7 Donor Back Transfer donor←donor

Since D_j has a probability $P_{D_j}^1(t)$ of being excited, then the probability that D_i remains excited will be increased for

$$W_{D_j^1}^{D_i^1}\left(R_{D_iD_j}\right)P_{D_i}^0(t)P_{D_j}^1(t) \tag{27}$$

This process is known as Donor Back Transfer (DBT) *donor* ← *donor*

An analogous situation occurs for an excited acceptor ion A_j once it gets excited. So, to

describe the probability of this ion to remain excited at time t, similar considerations have to be taken.

A simple schematization of the processes above described is shown in Figure 8, where the red spheres represent to the acceptors and the blue spheres represent the donors. In the figure it is shown how the ions A_1 and D_1 can give its energy to the neighboring ions or can relax by emitting a phonon

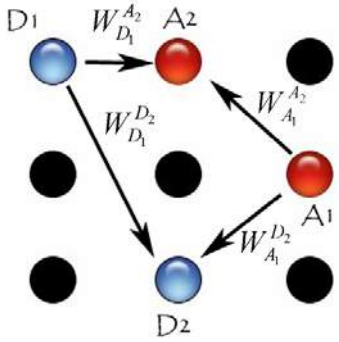

Figure 8 Forms that the ions can give its energy.

Then we can write the system of coupled equations that they govern the energy transfer processes among two level ions, as:

$$\frac{dP_{D_i}^1}{dt} = -\left[\frac{1}{\tau_{Do}} + \sum_{j=1}^{N_A} W_{D_i^1}^{A_j^1} P_{A_j}^0(t) + \sum_{j=1}^{N_D} W_{D_i^1}^{D_j^1} P_{D_j}^0(t)\right] P_{D_i}^1(t) + \left[\sum_{j=1}^{N_A} W_{A_j^1}^{D_i^1} P_{A_j}^1(t) + \sum_{j=1}^{N_D} W_{D_j^1}^{D_i^1} P_{D_j}^1(t)\right] P_{D_i}^0 \tag{28}$$

$$\frac{dP_{A_i}^1}{dt} = -\left[\frac{1}{\tau_{Ao}} + \sum_{j=1}^{N_A} W_{A_i^1}^{A_j^1} P_{A_j}^0(t) + \sum_{j=1}^{N_D} W_{A_i^1}^{D_j^1} P_{D_j}^0(t)\right] P_{A_i}^1(t) + \left[\sum_{j=1}^{N_A} W_{A_j^1}^{A_i^1} P_{A_j}^1(t) + \sum_{j=1}^{N_D} W_{D_j^1}^{A_i^1} P_{D_j}^1(t)\right] P_{A_i}^0 \tag{29}$$

The equations 28 and 29 govern in a general way the energy flow subject to transfer processes among two ion species, A and D. These equations represent a system of $N_A + N_D$ non linear coupled differential equations. Where in the equations 44 and 46, N_A is the total number of A ions in the crystal, N_D it is the total number of D ions that

are in the crystal. Remembering equations 15 and 16 we can eliminate the terms that involve the ground level for both types of ions:

$$\frac{dP_{D_i}}{dt} = -T_{D_i}^{D_i} P_{D_i} + \sum_{j=1}^{N_A} W_{A_j}^{D_i} P_{A_j} + \sum_{j=1}^{N_D} W_{D_j}^{D_i} P_{D_j} + \left[\sum_{j=1}^{N_A} \left(W_{D_i}^{A_j} - W_{A_j}^{D_i} \right) P_{A_j} \right] P_{D_i} \tag{30}$$

$$\frac{dP_{A_i}}{dt} = -T_{A_i}^{A_i} P_{A_i} + \sum_{j=1}^{N_A} W_{A_j}^{A_i} P_{A_j} + \sum_{j=1}^{N_A} W_{D_j}^{A_i} P_{D_j} + \left[\sum_{j=1}^{N_D} \left(W_{A_i}^{D_j} - W_{D_j}^{A_i} \right) P_{D_j} \right] P_{A_i} \tag{31}$$

Where

$$T_{D_i}^{D_i} = \frac{1}{\tau_{Do}} + \sum_{j=1}^{N_A} W_{D_i^1}^{A_j^1} + \sum_{j=1}^{N_D} W_{D_i^1}^{D_j^1} \tag{32}$$

$$T_{A_i}^{A_i} = \frac{1}{\tau_{Ao}} + \sum_{j=1}^{N_A} W_{A_i^1}^{A_j^1} + \sum_{j=1}^{N_D} W_{A_i^1}^{D_j^1} \tag{33}$$

This system of equations is still non linear and its non linearity depends critically on having, or not, resonance between the emission transition of the sensitizer and the absorption spectrum of the activator. This is explicitly reflected in the spectral overlap integral factor appearing in the expression for the energy-transfer rate. Phonons play an important role in ensuring the conservation of energy. For resonant electronic transition, phonons affect the widths of the spectral lines and thus the magnitude of spectral overlap integral. Also the temperature dependence of resonant energy transfer rates are contained in spectral overlap integrals.

We can see that equations 30 and 31 are equal to the GETME except for the last term that is related with the detuning between the direct transfer and the back transfer processes. Besides this last term is a non linear term of second order in P(t). So, from now on we refer to equations 30 and 31 as the Non linear General Energy Transfer Master Ecuations (NLGETME).

The NLGETME preserve their non linearlity for the case of non resonant energy levels, that is if

$$\int g_D^{EMISSION}(E)\, g_A^{ABSORTION}(E)\, dE \neq \int g_A^{EMISSION}(E)\, g_D^{ABSORTION}(E)\, dE \tag{34}$$

However, if

$$\int g_D^{EMISSION}(E)\, g_A^{ABSORTION}(E)\, dE = \int g_A^{EMISSION}(E)\, g_D^{ABSORTION}(E)\, dE \tag{35}$$

then the NLGETME become linear. In fact they reduce to the GETME system. That is due to the fact that for resonance conditions we have that:

$$W_{A_i}^{D_j} = W_{D_j}^{A_i} \tag{36}$$

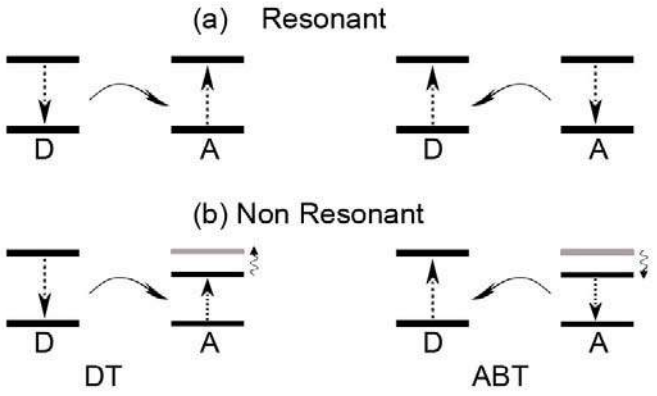

Figure 9 (a) Resonant case, (b) the non resonant

The resonant case is schematized in the figure 9a. This case is treated with more detail in Vega Durán Thesis. The non resonant case is schematized in the figure 9b. In this example the back transfer cannot be carried out since the acceptor would not have enough energy to excite the donor, the only form that this transition could be carried out it is to give additional energy to the material, for example to heat it to be able to broaden the energy levels. On the other side, the direct transfer can be carried out because the donor has more energy than the acceptor needs, and the difference would get lost in heat energy. As conclusion the last terms of NLGETME can be related with the increment or decrement of the temperature in the material.

4.1 Linearization

Our system of NLGETME can be rewritten [24] as

$$\dot{P} = f\left(P\right) \tag{37}$$

It is possible to approach $f(P)$ to a lineal system and to write it as

$$\dot{P} = KP \tag{38}$$

where the matrix $K = Df\left(P_{e,c}\right)$. The lineal function $KP = Df\left(P_{e,c}\right)P$ is known as the lineal part of f around $P_{e,c}$.

If $f : R^{N_A+N_D} \to R^{N_A+N_D}$ is derivable in $P_{e,c}$, then for every $P \in R^{N_A+N_D}$ exist

$$\frac{\partial f_i}{\partial P_j}, i, j = 1, ..., N_A + N_D \tag{39}$$

And the Jacovian is defined by,

$$Df = \left[\frac{\partial f_i}{\partial P_j}\right] \tag{40}$$

$$\left[\frac{\partial f_i}{\partial P_j}\right] = \begin{bmatrix} \frac{\partial f_1}{\partial P_{D_1}} & \cdots & \frac{\partial f_1}{\partial P_{D_{N_D}}} & \frac{\partial f_1}{\partial P_{A_1}} & \cdots & \frac{\partial f_1}{\partial P_{A_{N_A}}} \\ \vdots & \ddots & \vdots & \vdots & \ddots & \vdots \\ \frac{\partial f_{N_A+N_D}}{\partial P_{D_1}} & \cdots & \frac{\partial f_{N_A+N_D}}{\partial P_{D_{N_D}}} & \frac{\partial f_{N_A+N_D}}{\partial P_{A_1}} & \cdots & \frac{\partial f_{N_A+N_D}}{\partial P_{A_{N_A}}} \end{bmatrix} \tag{41}$$

Then from the Taylor Theorem

$$f\left(P\right) = f\left(P_{e,c}\right) + Df\left(P_{e,c}\right)\left(P - P_{e,c}\right) + \frac{1}{2}D^2 f\left(P_{e,c}\right)\left(P - P_{e,c}\right)^2 + ... \tag{42}$$

if we take only the first order, that its

$$f\left(P\right) = f\left(P_{e,c}\right) + Df\left(P_{e,c}\right)\left(P - P_{e,c}\right)$$

$$f\left(P\right) = f\left(P_o\right) + D\left[f\left(P\right)\right]_{P=P_o}\left(P - P_o\right)$$

$$= f(P_o) + D\left[f(P) \right]_{P=P_o} P - D\left[f(P) \right]_{P=P_o} P_o$$

$$= D\left[f(P) \right]_{P=P_o} P + f(P_o) - D\left[f(P) \right]_{P=P_o} P_o$$

From equations 30 and 31 we can write

$$f(P) = \begin{bmatrix} -T_{D_1}^{D_1} P_{D_1} + \sum_{j=1}^{N_A} W_{A_j}^{D_1} P_{A_j} + \sum_{j=1}^{N_D} W_{D_j}^{D_1} P_{D_j} \\ + \left[\sum_{j=1}^{N_A} \left(W_{D_1}^{A_j} - W_{A_j}^{D_1} \right) P_{A_j} \right] P_{D_1} \\ \vdots \\ -T_{D_{N_D}}^{D_{N_D}} P_{D_{N_D}} + \sum_{j=1}^{N_A} W_{A_j}^{D_{N_D}} P_{A_j} + \sum_{j=1}^{N_D} W_{D_j}^{D_{N_D}} P_{D_j} \\ + \left[\sum_{j=1}^{N_A} \left(W_{D_{N_D}}^{A_j} - W_{A_j}^{D_{N_D}} \right) P_{A_j} \right] P_{D_{N_D}} \\ -T_{A_1}^{A_1} P_{A_1} + \sum_{j=1}^{N_A} W_{A_j}^{A_1} P_{A_j} + \sum_{j=1}^{N_A} W_{D_j}^{A_1} P_{D_j} + \\ + \left[\sum_{j=1}^{N_D} \left(W_{A_1}^{D_j} - W_{D_j}^{A_1} \right) P_{D_j} \right] P_{A_1} \\ \vdots \\ -T_{A_{N_A}}^{A_{N_A}} P_{A_{N_A}} + \sum_{j=1}^{N_A} W_{A_j}^{A_{N_A}} P_{A_j} + \sum_{j=1}^{N_A} W_{D_j}^{A_{N_A}} P_{D_j} + \\ + \left[\sum_{j=1}^{N_D} \left(W_{A_{N_A}}^{D_j} - W_{D_j}^{A_{N_A}} \right) P_{D_j} \right] P_{A_{N_A}} \end{bmatrix} \quad (43)$$

The next step is calculate the derivatives $\frac{\partial f}{\partial P_{D_k}}$ and $\frac{\partial f}{\partial P_{A_l}}$.

Derivating f with regard to P_{D_k}

$$\frac{\partial f}{\partial P_{D_k}} = \begin{bmatrix} -T_{D_1}^{D_1}\delta_{P_{D_1}}^{P_{D_k}} + \sum_{j=1}^{N_A} W_{A_j}^{D_1}\delta_{P_{A_j}}^{P_{D_k}} + \sum_{j=1}^{N_D} W_{D_j}^{D_1}\delta_{P_{D_j}}^{P_{D_k}} \\ + \left[\sum_{j=1}^{N_A}\left(W_{D_1}^{A_j} - W_{A_j}^{D_1}\right)\delta_{P_{A_j}}^{P_{D_k}}\right] P_{D_1} \\ + \left[\sum_{j=1}^{N_A}\left(W_{D_1}^{A_j} - W_{A_j}^{D_1}\right) P_{A_j}\right]\delta_{P_{D_1}}^{P_{D_k}} \\ \vdots \\ -T_{D_{N_D}}^{D_{N_D}}\delta_{P_{D_{N_D}}}^{P_{D_k}} + \sum_{j=1}^{N_A} W_{A_j}^{D_{N_D}}\delta_{P_{A_j}}^{P_{D_k}} + \sum_{j=1}^{N_D} W_{D_j}^{D_{N_D}}\delta_{P_{D_j}}^{P_{D_k}} \\ + \left[\sum_{j=1}^{N_A}\left(W_{D_{N_D}}^{A_j} - W_{A_j}^{D_{N_D}}\right)\delta_{P_{A_j}}^{P_{D_k}}\right] P_{D_{N_D}} \\ \left[\sum_{j=1}^{N_A}\left(W_{D_{N_D}}^{A_j} - W_{A_j}^{D_{N_D}}\right) P_{A_j}\right]\delta_{P_{D_{N_D}}}^{P_{D_k}} \\ -T_{A_1}^{A_1}\delta_{P_{A_1}}^{P_{D_k}} + \sum_{j=1}^{N_A} W_{A_j}^{A_1}\delta_{P_{A_j}}^{P_{D_k}} + \sum_{j=1}^{N_A} W_{D_j}^{A_1}\delta_{P_{D_j}}^{P_{D_k}} + \\ + \left[\sum_{j=1}^{N_D}\left(W_{A_1}^{D_j} - W_{D_j}^{A_1}\right)\delta_{P_{D_j}}^{P_{D_k}}\right] P_{A_1} \\ + \left[\sum_{j=1}^{N_D}\left(W_{A_1}^{D_j} - W_{D_j}^{A_1}\right) P_{D_j}\right]\delta_{P_{A_1}}^{P_{D_k}} \\ \vdots \\ -T_{A_{N_A}}^{A_{N_A}}\delta_{P_{A_{N_A}}}^{P_{D_k}} + \sum_{j=1}^{N_A} W_{A_j}^{A_{N_A}}\delta_{P_{A_j}}^{P_{D_k}} + \sum_{j=1}^{N_A} W_{D_j}^{A_{N_A}}\delta_{P_{D_j}}^{P_{D_k}} + \\ + \left[\sum_{j=1}^{N_D}\left(W_{A_{N_A}}^{D_j} - W_{D_j}^{A_{N_A}}\right)\delta_{P_{D_j}}^{P_{D_k}}\right] P_{A_{N_A}} \\ + \left[\sum_{j=1}^{N_D}\left(W_{A_{N_A}}^{D_j} - W_{D_j}^{A_{N_A}}\right) P_{D_j}\right]\delta_{P_{A_{N_A}}}^{P_{D_k}} \end{bmatrix} \tag{44}$$

or

$$\frac{\partial f}{\partial P_{D_k}} = \begin{bmatrix} -T_{D_1}^{D_1}\delta_{P_{D_1}}^{P_{D_k}} + \sum_{j=1}^{N_D} W_{D_j}^{D_1}\delta_{P_{D_j}}^{P_{D_k}} \\ \vdots \\ -T_{D_{N_D}}^{D_{N_D}}\delta_{P_{D_{N_D}}}^{P_{D_k}} + \sum_{j=1}^{N_D} W_{D_j}^{D_{N_D}}\delta_{P_{D_j}}^{P_{D_k}} \\ \sum_{j=1}^{N_A} W_{D_j}^{A_1}\delta_{P_{D_j}}^{P_{D_k}} \\ \vdots \\ \sum_{j=1}^{N_A} W_{D_j}^{A_{N_A}}\delta_{P_{D_j}}^{P_{D_k}} \end{bmatrix} + \begin{bmatrix} \left[\sum_{j=1}^{N_A}\left(W_{D_1}^{A_j} - W_{A_j}^{D_1}\right) P_{A_j}\right]\delta_{P_{D_1}}^{P_{D_k}} \\ \vdots \\ \left[\sum_{j=1}^{N_A}\left(W_{D_{N_D}}^{A_j} - W_{A_j}^{D_{N_D}}\right) P_{A_j}\right]\delta_{P_{D_{N_D}}}^{P_{D_k}} \\ \left[\sum_{j=1}^{N_D}\left(W_{A_1}^{D_j} - W_{D_j}^{A_1}\right)\delta_{P_{D_j}}^{P_{D_k}}\right] P_{A_1} \\ \vdots \\ \left[\sum_{j=1}^{N_D}\left(W_{A_{N_A}}^{D_j} - W_{D_j}^{A_{N_A}}\right)\delta_{P_{D_j}}^{P_{D_k}}\right] P_{A_{N_A}} \end{bmatrix}$$

for $k = 1,...,N_D$. Then we need to evaluate $\frac{\partial f}{\partial P_{D_k}}$ in P_o

$$\left(\frac{\partial f}{\partial P_{D_k}}\right)_{P=P_o} = \begin{bmatrix} -T_{D_1}^{D_1}\delta_{P_{D_1}}^{P_{D_k}} + \sum_{j=1}^{N_D} W_{D_j}^{D_1}\delta_{P_{D_j}}^{P_{D_k}} \\ \vdots \\ -T_{D_{N_D}}^{D_{N_D}}\delta_{P_{D_{N_D}}}^{P_{D_k}} + \sum_{j=1}^{N_D} W_{D_j}^{D_{N_D}}\delta_{P_{D_j}}^{P_{D_k}} \\ \sum_{j=1}^{N_A} W_{D_j}^{A_1}\delta_{P_{D_j}}^{P_{D_k}} \\ \vdots \\ \sum_{j=1}^{N_A} W_{D_j}^{A_{N_A}}\delta_{P_{D_j}}^{P_{D_k}} \end{bmatrix} \tag{45}$$

Derivating f with regard to P_{A_1}

$$\frac{\partial f}{\partial P_{A_l}} = \begin{bmatrix} -T_{D_1}^{D_1}\delta_{P_{D_1}}^{P_{A_l}} + \sum_{j=1}^{N_A} W_{A_j}^{D_1}\delta_{P_{A_j}}^{P_{A_l}} + \sum_{j=1}^{N_D} W_{D_j}^{D_1}\delta_{P_{D_j}}^{P_{A_l}} \\ + \left[\sum_{j=1}^{N_A}\left(W_{D_1}^{A_j} - W_{A_j}^{D_1}\right)\delta_{P_{A_j}}^{P_{A_l}}\right] P_{D_1} \\ + \left[\sum_{j=1}^{N_A}\left(W_{D_1}^{A_j} - W_{A_j}^{D_1}\right) P_{A_j}\right]\delta_{P_{D_1}}^{P_{A_l}} \\ \vdots \\ -T_{D_{N_D}}^{D_{N_D}}\delta_{P_{D_{N_D}}}^{P_{A_l}} + \sum_{j=1}^{N_A} W_{A_j}^{D_{N_D}}\delta_{P_{A_j}}^{P_{A_l}} + \sum_{j=1}^{N_D} W_{D_j}^{D_{N_D}}\delta_{P_{D_j}}^{P_{A_l}} \\ + \left[\sum_{j=1}^{N_A}\left(W_{D_{N_D}}^{A_j} - W_{A_j}^{D_{N_D}}\right)\delta_{P_{A_j}}^{P_{A_l}}\right] P_{D_{N_D}} \\ + \left[\sum_{j=1}^{N_A}\left(W_{D_{N_D}}^{A_j} - W_{A_j}^{D_{N_D}}\right) P_{A_j}\right]\delta_{P_{D_{N_D}}}^{P_{A_l}} \\ -T_{A_1}^{A_1}\delta_{P_{A_1}}^{P_{A_l}} + \sum_{j=1}^{N_A} W_{A_j}^{A_1}\delta_{P_{A_j}}^{P_{A_l}} + \sum_{j=1}^{N_A} W_{D_j}^{A_1}\delta_{P_{D_j}}^{P_{A_l}} + \\ + \left[\sum_{j=1}^{N_D}\left(W_{A_1}^{D_j} - W_{D_j}^{A_1}\right)\delta_{P_{D_j}}^{P_{A_l}}\right] P_{A_1} \\ + \left[\sum_{j=1}^{N_D}\left(W_{A_1}^{D_j} - W_{D_j}^{A_1}\right) P_{D_j}\right]\delta_{P_{A_1}}^{P_{A_l}} \\ \vdots \\ -T_{A_{N_A}}^{A_{N_A}}\delta_{P_{A_{N_A}}}^{P_{A_l}} + \sum_{j=1}^{N_A} W_{A_j}^{A_{N_A}}\delta_{P_{A_j}}^{P_{A_l}} + \sum_{j=1}^{N_A} W_{D_j}^{A_{N_A}}\delta_{P_{D_j}}^{P_{A_l}} + \\ + \left[\sum_{j=1}^{N_D}\left(W_{A_{N_A}}^{D_j} - W_{D_j}^{A_{N_A}}\right)\delta_{P_{D_j}}^{P_{A_l}}\right] P_{A_{N_A}} \\ + \left[\sum_{j=1}^{N_D}\left(W_{A_{N_A}}^{D_j} - W_{D_j}^{A_{N_A}}\right) P_{D_j}\right]\delta_{P_{A_{N_A}}}^{P_{A_l}} \end{bmatrix}$$

for $l = 1, \ldots, N_A$

$$\frac{\partial f}{\partial P_{A_l}} = \begin{bmatrix} \sum_{j=1}^{N_A} W_{A_j}^{D_1}\delta_{P_{A_j}}^{P_{A_l}} \\ \vdots \\ \sum_{j=1}^{N_A} W_{A_j}^{D_{N_D}}\delta_{P_{A_j}}^{P_{A_l}} \\ -T_{A_1}^{A_1}\delta_{P_{A_1}}^{P_{A_l}} + \sum_{j=1}^{N_A} W_{A_j}^{A_1}\delta_{P_{A_j}}^{P_{A_l}} \\ \vdots \\ -T_{A_{N_A}}^{A_{N_A}}\delta_{P_{A_{N_A}}}^{P_{A_l}} + \sum_{j=1}^{N_A} W_{A_j}^{A_{N_A}}\delta_{P_{A_j}}^{P_{A_l}} \end{bmatrix} + \begin{bmatrix} \left[\sum_{j=1}^{N_A}\left(W_{D_1}^{A_j} - W_{A_j}^{D_1}\right)\delta_{P_{A_j}}^{P_{A_l}}\right] P_{D_1} \\ \vdots \\ \left[\sum_{j=1}^{N_A}\left(W_{D_{N_D}}^{A_j} - W_{A_j}^{D_{N_D}}\right)\delta_{P_{A_j}}^{P_{A_l}}\right] P_{D_{N_D}} \\ \left[\sum_{j=1}^{N_D}\left(W_{A_1}^{D_j} - W_{D_j}^{A_1}\right) P_{D_j}\right]\delta_{P_{A_1}}^{P_{A_l}} \\ \vdots \\ \left[\sum_{j=1}^{N_D}\left(W_{A_{N_A}}^{D_j} - W_{D_j}^{A_{N_A}}\right) P_{D_j}\right]\delta_{P_{A_{N_A}}}^{P_{A_l}} \end{bmatrix}$$

$$\left(\frac{\partial f}{\partial P_{A_l}}\right)_{P=P_o} = \begin{bmatrix} \sum_{j=1}^{N_A} W_{A_j}^{D_1}\delta_{P_{A_j}}^{P_{A_l}} \\ \vdots \\ \sum_{j=1}^{N_A} W_{A_j}^{D_{N_D}}\delta_{P_{A_j}}^{P_{A_l}} \\ -T_{A_l}^{A_1}\delta_{P_{A_l}}^{P_{A_l}} + \sum_{j=1}^{N_A} W_{A_j}^{A_l}\delta_{P_{A_j}}^{P_{A_l}} \\ \vdots \\ -T_{A_{N_A}}^{A_{N_A}}\delta_{P_{A_{N_A}}}^{P_{A_l}} + \sum_{j=1}^{N_A} W_{A_j}^{A_{N_A}}\delta_{P_{A_j}}^{P_{A_l}} \end{bmatrix} + \begin{bmatrix} \left[\sum_{j=1}^{N_A}\left(W_{D_1}^{A_j} - W_{A_j}^{D_1}\right)\delta_{P_{A_j}}^{P_{A_l}}\right] \\ \vdots \\ \left[\sum_{j=1}^{N_A}\left(W_{D_{N_D}}^{A_j} - W_{A_j}^{D_{N_D}}\right)\delta_{P_{A_j}}^{P_{A_l}}\right] \\ \left[\sum_{j=1}^{N_D}\left(W_{A_l}^{D_j} - W_{D_j}^{A_1}\right)\right]\delta_{P_{A_l}}^{P_{A_l}} \\ \vdots \\ \left[\sum_{j=1}^{N_D}\left(W_{A_{N_A}}^{D_j} - W_{D_j}^{A_{N_A}}\right)\right]\delta_{P_{A_{N_A}}}^{P_{A_l}} \end{bmatrix}$$

Finally

$$D\left[f(P)\right]_{P=P_o} = W + K' \tag{46}$$

$$W = \begin{bmatrix} -T_{D_1}^{D_1} & \cdots & W_{D_{N_D}}^{D_1} & W_{A_l}^{D_1} & \cdots & W_{A_{N_A}}^{D_1} \\ \vdots & \ddots & \vdots & \vdots & \ddots & \vdots \\ W_{D_1}^{D_{N_D}} & \cdots & -T_{D_{N_D}}^{D_{N_D}} & W_{A_l}^{D_{N_D}} & \cdots & W_{A_{N_A}}^{D_{N_D}} \\ W_{D_1}^{A_l} & \cdots & W_{D_{N_D}}^{A_l} & -T_{A_l}^{A_l} & \cdots & W_{A_{N_A}}^{A_{N_A}} \\ \vdots & \ddots & \vdots & \vdots & \ddots & \vdots \\ W_{D_1}^{A_{N_A}} & \cdots & W_{D_{N_D}}^{A_{N_A}} & W_{A_l}^{A_{N_A}} & \cdots & -T_{A_{N_A}}^{A_{N_A}} \end{bmatrix} \tag{47}$$

$$K' = \begin{bmatrix} 0 & \cdots & 0 & W_{D_1}^{A_l} - W_{A_l}^{D_1} & \cdots & W_{D_1}^{A_{N_A}} - W_{A_{N_A}}^{D_1} \\ \vdots & \ddots & \vdots & \vdots & \ddots & \vdots \\ 0 & \cdots & 0 & W_{D_{N_D}}^{A_l} - W_{A_l}^{D_{N_D}} & \cdots & W_{D_{N_D}}^{A_{N_A}} - W_{A_{N_A}}^{D_{N_D}} \\ 0 & \cdots & 0 & \sum_{j=1}^{N_D}\left(W_{A_l}^{D_j} - W_{D_j}^{A_l}\right) & \cdots & 0 \\ \vdots & \ddots & \vdots & \vdots & \ddots & \vdots \\ 0 & \cdots & 0 & 0 & \cdots & \sum_{j=1}^{N_D}\left(W_{A_{N_A}}^{D_j} - W_{D_j}^{A_{N_A}}\right) \end{bmatrix} \tag{48}$$

Remembering that our equation to solve is

$$\frac{dP}{dt} = D\left[f\left(P\right)\right]_{P=P_o} P + f\left(P_o\right) - D\left[f\left(P\right)\right]_{P=P_o} P_o \tag{49}$$

Let us simplify $f\left(P_o\right) - D\left[f\left(P\right)\right]_{P=P_o} P_o$

$$D\left[f\left(P\right)\right]_{P=P_o} P_o = \begin{bmatrix} -T_{D_1}^{D_1} & \cdots & W_{D_{N_D}}^{D_1} & W_{A_1}^{D_1} & \cdots & W_{A_{N_A}}^{D_1} \\ \vdots & \ddots & \vdots & \vdots & \ddots & \vdots \\ W_{D_1}^{D_{N_D}} & \cdots & -T_{D_{N_D}}^{D_{N_D}} & W_{A_1}^{D_{N_D}} & \cdots & W_{A_{N_A}}^{D_{N_D}} \\ W_{D_1}^{A_1} & \cdots & W_{D_{N_D}}^{A_1} & -T_{A_1}^{A_1} & \cdots & W_{A_{N_A}}^{A_{N_A}} \\ \vdots & \ddots & \vdots & \vdots & \ddots & \vdots \\ W_{D_1}^{A_{N_A}} & \cdots & W_{D_{N_D}}^{A_{N_A}} & W_{A_1}^{A_{N_A}} & \cdots & -T_{A_{N_A}}^{A_{N_A}} \end{bmatrix} \begin{bmatrix} 1 \\ \vdots \\ 1 \\ 0 \\ \vdots \\ 0 \end{bmatrix} =$$

$$= \begin{bmatrix} -T_{D_1}^{D_1} + \sum_{j=1}^{N_D} W_{D_j}^{D_1} \\ \vdots \\ -T_{D_{N_D}}^{D_{N_D}} + \sum_{j=1}^{N_D} W_{D_j}^{D_{N_D}} \\ \sum_{j=1}^{N_D} W_{D_j}^{A_1} \\ \vdots \\ \sum_{j=1}^{N_D} W_{D_j}^{A_{N_A}} \end{bmatrix}$$

and

$$f\left(P_o\right) = \begin{bmatrix} -T_{D_1}^{D_1} + \sum_{j=1}^{N_D} W_{D_j}^{D_1} \\ \vdots \\ -T_{D_{N_D}}^{D_{N_D}} + \sum_{j=1}^{N_D} W_{D_j}^{D_{N_D}} \\ \sum_{j=1}^{N_A} W_{D_j}^{A_1} \\ \vdots \\ \sum_{j=1}^{N_A} W_{D_j}^{A_{N_A}} \end{bmatrix} \text{ and}$$

$$f(P_o) - D\left[f(P) \right]_{P=P_o} P_o = \begin{bmatrix} -T_{D_1}^{D_1} + \sum_{j=1}^{N_D} W_{D_j}^{D_1} \\ \vdots \\ -T_{D_{N_D}}^{D_{N_D}} + \sum_{j=1}^{N_D} W_{D_j}^{D_{N_D}} \\ \sum_{j=1}^{N_A} W_{D_j}^{A_1} \\ \vdots \\ \sum_{j=1}^{N_A} W_{D_j}^{A_{N_A}} \end{bmatrix} + \begin{bmatrix} T_{D_1}^{D_1} - \sum_{j=1}^{N_D} W_{D_j}^{D_1} \\ \vdots \\ T_{D_{N_D}}^{D_{N_D}} - \sum_{j=1}^{N_D} W_{D_j}^{D_{N_D}} \\ -\sum_{j=1}^{N_D} W_{D_j}^{A_1} \\ \vdots \\ -\sum_{j=1}^{N_D} W_{D_j}^{A_{N_A}} \end{bmatrix} = \begin{bmatrix} 0 \\ \vdots \\ 0 \\ 0 \\ \vdots \\ 0 \end{bmatrix}$$

Thus the final first order approximation to $\dot{P} = f(P)$ is given by,

$$\frac{dP}{dt} = D\left[f(P) \right]_{P=P_o} P \tag{50}$$

where $D\left[f(P) \right]_{P=P_o} = K = W + K'$, this equations are called LNLGETME. One can observe that this is in fact an Linear homogeneous set of coupled differential eqs. and its solution is of the form :

$$P = e^{tK} P_o$$

Notice that this solution has the same algebraic form that the solution for the GETME, so the evaluation of this more general solution follows the same numerical implementation as described in appendix A. Therefore the LNLGETME can give us a second approximation to the experimental decay of both Donor ans acceptor, and again, the comparison between the LNLGETME and the experimental measurements leads to the microinteraction parameters of the interactions reposnsible for the energy transfer processes taking place in the studied luminescent crystal.

For example if we considerate a imaginary nanocrystal with 20% monoclinic phase, 80% tetragonal phase, mean diameter 9.7141nm,we considerate only direct transfer between donors and dipole-dipole interaction R_{06} = 6 A. In figure 10, we apply GETME and LNLGETME. In the figure 10A we can see the non resonant case. For a slow donor and acceptor concentration both systems solutions are similar but if we increase donor and acceptor concentration those systems are different. In GETME, the effect quenching

concentration is stronger than LNLGETME. This means that if we want to have similar lifetime the LNLGETME dipole-dipole interaction must to be bigger than GETME dipole-dipole interaction. In conclusion the non resonant energy level is very important to solve the quenching concentration. In the figure 10B we can see the resonant case, for this example both solutions (GETME and LNLGETME) are equal.

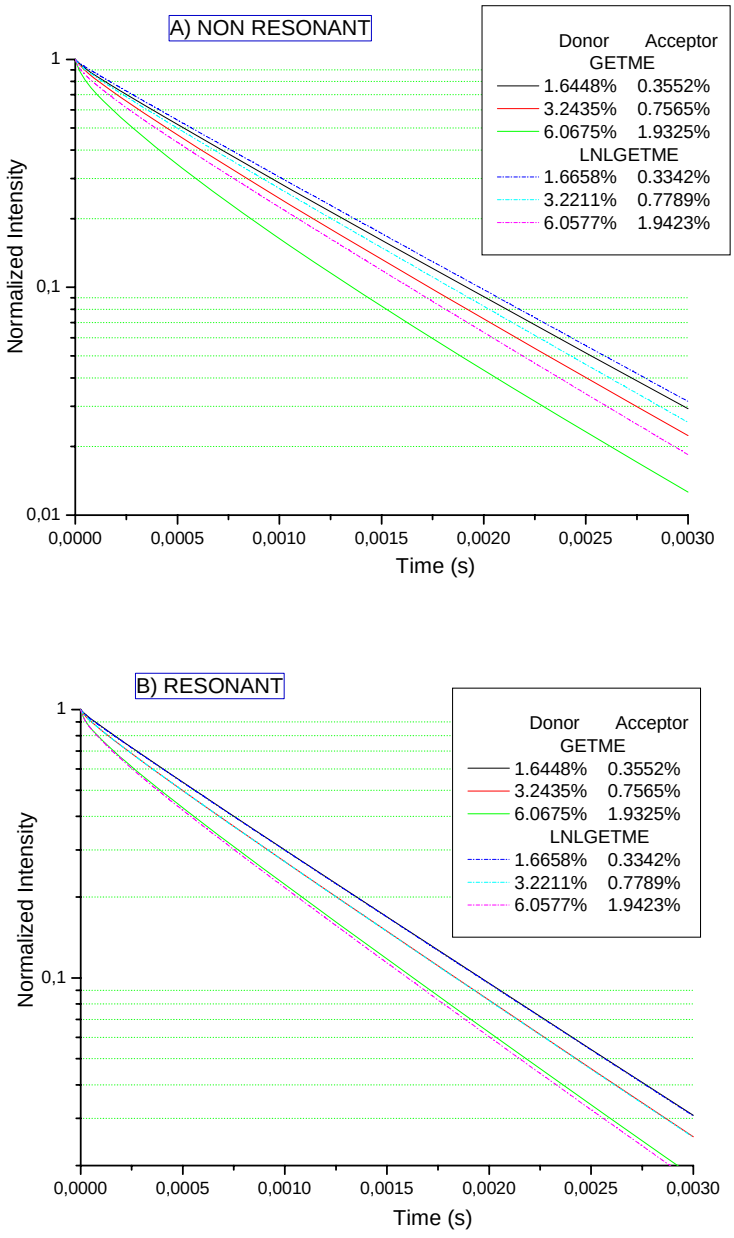

Figure 10 a) GETME and b) LNLGETME simulation

5. Non radiative energy transfer between two and three level ions The General Energy Transfer Upconversion Equations (GETUPE):

Let us consider that the acceptors ions have three energy levels, that is to say, the ground state $\left(A^0\right)$, and two excited levels $\left(A^1\right)$ and $\left(A^2\right)$. The donor has only two levels of energy, the ground state $\left(D^0\right)$, and the excited level $\left(D^1\right)$.

The D and A ions are distributed in the possible places of the crystalline lattice and they are separated by a distance $R_{D_iA_j}$. It considered that $R_{D_iA_j}$ is a discreet aleatory variable that depends on the dopants concentration as well as the crystalline phase of the material.

Let us consider that the i-th donor is excited in t=0 and it can transfer its energy to another ion inside the crystal. It is convenient to define $P_{A_j}^2\left(t\right)$ as is the individual probability of the j-th acceptor to remain excited at the time t in second excited energy level these probabilities should fulfill that

$$P_{A_j}^2\left(t\right)+P_{A_j}^1\left(t\right)+P_{A_j}^0\left(t\right)=1 \tag{51}$$

$$P_{D_j}^1\left(t\right)+P_{D_j}^0\left(t\right)=1 \tag{52}$$

Next we will show some interactions that involve the second level of the Acceptors ions.

1.- The i-th donor can non radiatively transfer its energy to a j-th acceptor that is its first excited energy level at a distance $R_{D_iA_j}$ with a transfer rate,see fig 11a

$$W_{D_i^1}^{A_j^2}\left(R_{D_iA_j}\right)$$

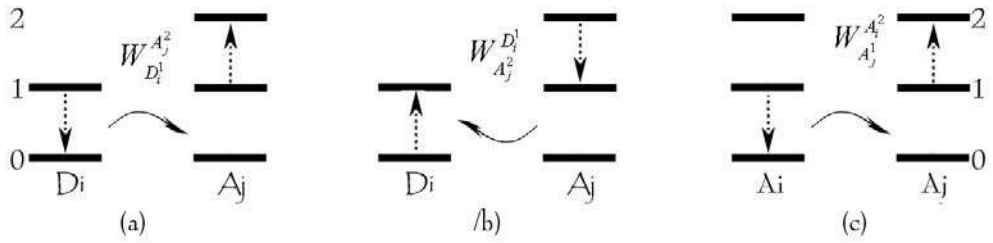

Figure 11(a) Upconvertion (UC) donor→acceptor² , (b) Down conversion by cross relaxation from acceptor to donor donor←acceptor², (c) Upconversion from acceptor to acceptor acceptor←acceptor²

Thus the decrement of the individual probability of the i-th donor is the product of the transfer rate by the probability that the ion D_i is excited $P_{D_i}^1(t)$ and that the ion A_j is in the first state $P_{A_j}^1(t)$, that is to say

$$W_{D_i^1}^{A_j^2}\left(R_{D_iA_j}\right)P_{D_i}^1(t)P_{A_j}^1(t)$$

this is a energy transfer driven upconversion process, This process is known as Upconvertion (UC) or $donant \rightarrow acceptor^2$.

2.- The i-th donor at its ground level can receive energy from a j-th acceptor in the excited energy level at a distance $R_{D_iA_j}$ with a transfer rate (see fig 11b):

$$W_{A_j^2}^{D_i^1}\left(R_{D_iA_j}\right)$$

The probability is

$$W_{A_j^2}^{D_i^1}\left(R_{D_iA_j}\right)P_{D_i}^0P_{A_j}^2$$

this is a cross relaxation process.

3.- The i-th acceptor in the first level can non radiatively transfer its energy to a j-th acceptor in the first level energy at a distance $R_{D_iA_j}$ with a rate changes given by: (see fig 11c):

$$W_{A_i^1}^{A_j^2}\left(R_{A_iA_j}\right)P_{A_i}^1P_{A_j}^1$$

4.- All the processes that involve the increment of probability for excited energy level

of the acceptor are schematized in the figure 12, they have the rate changes given by::

$$W_{A_j^2}^{A_i^1}\left(R_{A_iA_j}\right)P_{A_i}^0P_{A_j}^2$$

$$W_{A_i^2}^{A_j^2}\left(R_{A_iA_j}\right)P_{A_i}^2P_{A_j}^1$$

$$W_{A_i^2}^{D_j^1}\left(R_{A_iA_j}\right)P_{A_i}^2P_{D_j}^0$$

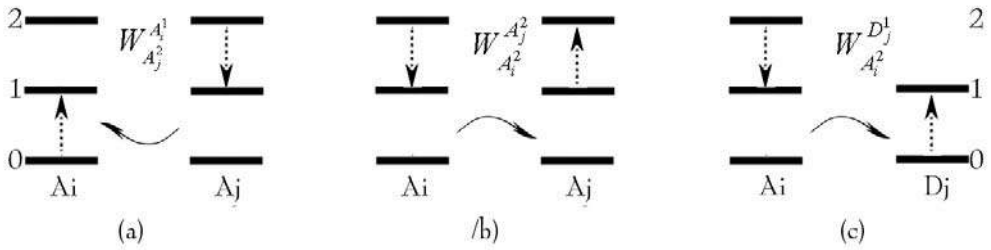

Figure 12 Forms in that the level one of the aceptor A_i you can receive energy due to the introduction of a third energy level to the acepptors.

5.- The acceptor in the second energy level can lose his energy in the ways schematized in the figure 13, they have the probability:

$$\frac{1}{\tau_A^2}P_{A_i}^2$$

$$W_{A_i^2}^{A_j^1}\left(R_{A_iA_j}\right)P_{A_i}^2P_{A_j}^0$$

$$W_{A_i^2}^{D_j^1}\left(R_{A_iD_j}\right)P_{A_i}^2P_{D_j}^0$$

$$W_{A_i^2}^{A_j^2}\left(R_{A_iA_j}\right)P_{A_i}^2P_{A_j}^1$$

$$\hat{W}_{A_i^2}^{A_j^2}\left(R_{A_iA_j}\right)P_{A_i}^2P_{A_j}^0$$

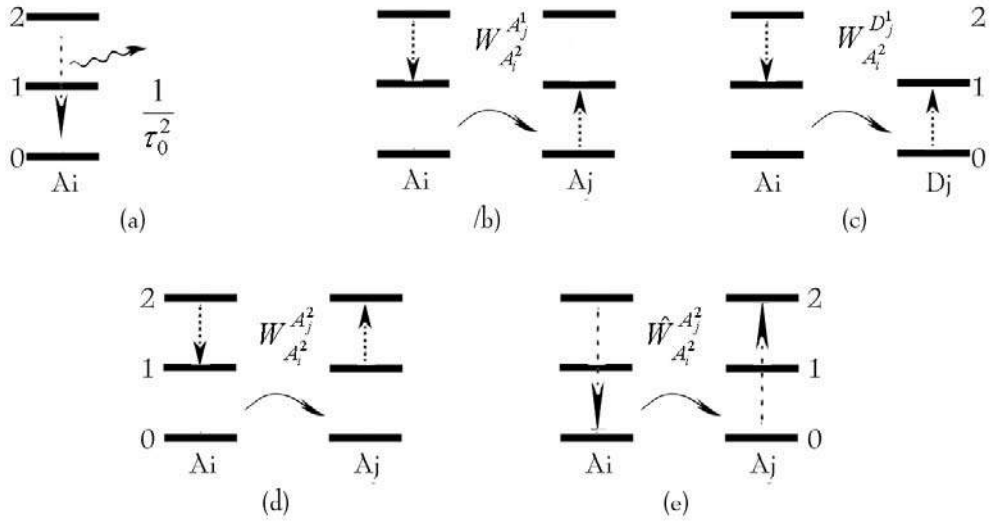

Figure 13 The acepptor in the second energy level can lose his energy in these ways

6.- The acceptor can win energy and to be promoted at the second energy level in the ways schematized in the figure 14, they have the rate changes given by:

$$W_{D_j^1}^{A_i^2}\left(R_{A_iD_j}\right)P_{D_j}^1P_{A_i}^1$$

$$W_{A_j^1}^{A_i^2}\left(R_{A_iA_j}\right)P_{A_j}^1P_{A_i}^1$$

$$W_{A_j^2}^{A_i^2}\left(R_{A_iA_j}\right)P_{A_j}^2P_{A_i}^1$$

$$\hat{W}_{A_j^2}^{A_i^2}\left(R_{A_iA_j}\right)P_{A_j}^2P_{A_i}^0$$

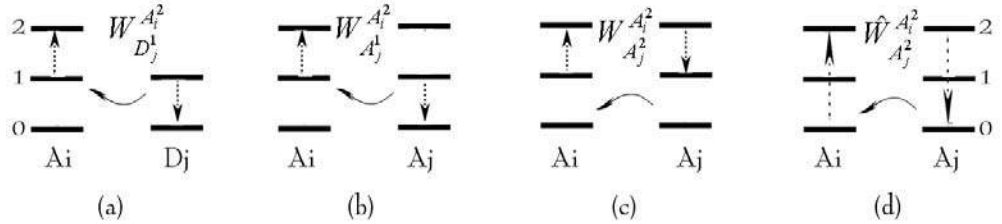

Figure 14 The ion A_i it can win energy in the following ways

Then we can write the system of coupled equations that they govern the Non radiative energy transfer between two and three (NLGETME23) level ions (Upconversion), as:

$$\frac{dP_{D_i}^0}{dt} = \begin{bmatrix} \frac{1}{\tau_{D_1^0}} P_{D_i}^1 + \begin{pmatrix} \sum W_{D_i^1}^{D_j^1} P_{D_j^0} \\ \sum \left(W_{D_i^1}^{A_j^1} P_{A_j^0} + W_{D_i^1}^{A_j^2} P_{A_j^1} \right) \end{pmatrix} P_{D_i^1} + \\ -\sum W_{A_j^2}^{D_i^1} P_{D_i}^0 P_{A_j^2} - \sum W_{D_j^1}^{D_i^1} P_{D_i}^0 P_{D_j^1} - \sum W_{A_j^1}^{D_i^1} P_{D_i}^0 P_{A_j^1} \end{bmatrix}$$

$$\frac{dP_{D_i}^1}{dt} = \begin{pmatrix} -\frac{1}{\tau_{D_1^0}} P_{D_i}^1 - \begin{bmatrix} \sum W_{D_i^1}^{D_j^1} P_{D_j}^0 \\ \sum \left(W_{D_i^1}^{A_j^1} P_{A_j}^0 + W_{D_i^1}^{A_j^2} P_{A_j}^1 \right) \end{bmatrix} P_{D_i}^1 \\ + \sum W_{D_j^1}^{D_i^1} P_{D_j}^1 P_{D_i}^0 + \sum W_{A_j^1}^{D_i^1} P_{A_j}^1 P_{D_i}^0 \end{pmatrix}$$

$$\frac{dP_{A_i}^0}{dt} = \begin{bmatrix} \frac{1}{\tau_{A_1^0}} P_{A_i}^1 + \frac{1}{\tau_{A_2^0}} P_{A_i}^2 + \begin{pmatrix} \sum \left(W_{A_i^1}^{A_j^1} P_{A_j^0} + W_{A_i^1}^{A_j^2} P_{A_j^1} \right) \\ \sum W_{A_i^1}^{D_j^1} P_{D_j^0} \end{pmatrix} P_{A_i^1} + \sum W_{A_i^2}^{A_j^2} P_{A_j^0} P_{A_i^2} \\ -\sum W_{A_j^2}^{A_i^1} P_{A_i}^0 P_{A_j^2} - \sum W_{A_j^1}^{A_i^1} P_{A_i}^0 P_{A_j^1} - \sum W_{D_j^1}^{A_i^1} P_{A_i}^0 P_{D_j^1} \end{bmatrix}$$

$$\frac{dP_{A_i}^1}{dt} = \begin{pmatrix} -\frac{1}{\tau_{A_1^0}} P_{A_i}^1 - \begin{bmatrix} \sum \left(W_{A_i^1}^{A_j^1} P_{A_j}^0 + \left(W_{A_i^1}^{A_j^2} + W_{A_j^1}^{A_i^2} \right) P_{A_j}^1 + \hat{W}_{A_j^2}^{A_i^2} P_{A_j}^2 \right) + \\ + \sum \left(W_{A_i^1}^{D_j^1} P_{D_j}^0 + W_{D_j^1}^{A_i^2} P_{D_j}^1 \right) \end{bmatrix} P_{A_i}^1 + \\ + \begin{bmatrix} \sum \left(W_{A_i^2}^{A_j^1} P_{A_i}^2 P_{A_j}^0 + \hat{W}_{A_i^2}^{A_j^2} P_{A_i}^2 P_{A_j}^1 + W_{A_j^1}^{A_i^1} P_{A_j}^1 P_{A_i}^0 + W_{A_j^2}^{A_i^1} P_{A_j}^2 P_{A_i}^0 \right) + \\ + \sum \left(W_{A_i^2}^{D_j^1} P_{A_i}^2 P_{D_j}^0 + W_{D_j^1}^{A_i^1} P_{D_j}^1 P_{A_i}^0 \right) \end{bmatrix} + \\ + \frac{1}{\tau_{A_2^1}} P_{A_i}^2 \end{pmatrix}$$

$$\frac{dP_{A_i}^2}{dt} = \left(-\frac{1}{\tau_{A_2^1}} P_{A_i}^2 - \frac{1}{\tau_{A_2^0}} P_{A_i}^2 - \left[\sum \left(W_{A_i^2}^{A_j^1} P_{A_j}^0 + \hat{W}_{A_i^2}^{A_j^2} P_{A_j}^1 + W_{A_i^2}^{A_j^2} P_{A_j}^0 \right) + \sum W_{A_i^2}^{D_j^1} P_{D_j}^0 \right] P_{A_i}^2 + \left[\sum \left(W_{A_j^1}^{A_i^2} P_{A_j}^1 P_{A_i}^1 + \hat{W}_{A_j^2}^{A_i^2} P_{A_j}^2 P_{A_i}^1 + W_{A_j^2}^{A_i^2} P_{A_j}^2 P_{A_i}^0 \right) + \sum W_{D_j^1}^{A_i^2} P_{D_j}^1 P_{A_i}^1 \right] \right)$$

It is convenient to eliminate the probabilities of the ground levels of the ions using the relationships 51 and 52, to obtain:

$$\frac{dP_{D_i}^1}{dt} = \left(-\frac{1}{\tau_{D_1^0}} P_{D_i}^1 - \left[\sum W_{D_i^1}^{D_j^1} + \sum W_{D_i^1}^{A_j^1} \right] P_{D_i}^1 + \sum \left[W_{D_j^1}^{D_i^1} P_{D_j}^1 \right] + \sum \left[W_{A_j^1}^{D_i^1} P_{A_j}^1 + W_{A_j^2}^{D_i^1} P_{A_j}^2 \right] + \sum \left(\left[W_{D_i^1}^{A_j^1} - W_{A_j^1}^{D_i^1} \right] P_{A_j}^1 + \left[W_{D_i^1}^{A_j^1} - W_{A_j^2}^{D_i^1} \right] P_{A_j}^2 \right) P_{D_i}^1 \right)$$

$$\frac{dP_{A_i}^1}{dt} = \left(\begin{array}{c} -\frac{1}{\tau_{A_1^0}} P_{A_i}^1 - \left[\sum W_{A_i^1}^{A_j^1} + \sum W_{A_i^1}^{D_j^1} \right] P_{A_i}^1 + \frac{1}{\tau_{A_2^1}} P_{A_i}^2 \\ + \sum \left[W_{A_i^2}^{A_j^1} P_{A_i}^2 + W_{A_j^1}^{A_i^1} P_{A_j}^1 + W_{A_j^2}^{A_i^1} P_{A_j}^2 \right] + \sum \left[W_{A_i^2}^{D_j^1} P_{A_i}^2 + W_{D_j^1}^{A_i^1} P_{D_j}^1 \right] \\ + \left[\begin{array}{c} \sum \left(\left[W_{A_i^1}^{A_j^1} - W_{A_j^2}^{A_i^1} - \hat{W}_{A_j^2}^{A_i^2} \right] P_{A_j}^2 \right) + \\ + \sum \left(\left[W_{A_i^1}^{D_j^1} - W_{D_j^1}^{A_i^1} - W_{D_j^1}^{A_i^2} \right] P_{D_j}^1 \right) \end{array} \right] P_{A_i}^1 + \\ + \sum \left[\begin{array}{c} \left(\hat{W}_{A_i^2}^{A_j^2} - W_{A_i^2}^{A_j^1} - W_{A_j^1}^{A_i^1} \right) P_{A_j}^1 + \\ + \left(-W_{A_i^2}^{A_j^1} - W_{A_j^2}^{A_i^1} \right) P_{A_j}^2 \end{array} \right] P_{A_i}^2 + \\ + \sum \left[\left(-W_{A_i^2}^{D_j^1} - W_{D_j^1}^{A_i^1} \right) P_{D_j}^1 \right] P_{A_i}^2 \end{array} \right)$$

$$\frac{dP_{A_i}^2}{dt} = \left(\begin{array}{c} -\left(\frac{1}{\tau_{A_2^1}} + \frac{1}{\tau_{A_2^0}} \right) P_{A_i}^2 - \left[\sum \left[W_{A_i^2}^{A_j^1} + W_{A_i^2}^{A_j^2} \right] + \sum W_{A_i^2}^{D_j^1} \right] P_{A_i}^2 \\ + \sum W_{A_j^2}^{A_i^2} P_{A_j}^2 + \left[\sum W_{A_j^1}^{A_i^2} P_{A_j}^1 + \sum W_{D_j^1}^{A_i^2} P_{D_j}^1 \right] P_{A_i}^1 \\ + \left[\sum \left(\left[-\hat{W}_{A_i^2}^{A_j^2} + W_{A_i^2}^{A_j^1} + W_{A_i^2}^{A_j^2} \right] P_{A_j}^1 + W_{A_i^2}^{A_j^1} P_{A_j}^2 \right) + \sum W_{A_i^2}^{D_j^1} P_{D_j}^1 \right] P_{A_i}^2 \end{array} \right)$$

where

$$T_{D_i^1}^1 = \frac{1}{\tau_{D_1^0}} + \left[\sum W_{D_i^1}^{D_j^1} + \sum W_{D_i^1}^{A_j^1} \right]$$

$$T^{1}_{A^{1}_{i}} = \frac{1}{\tau_{A^{0}_{1}}} + \left[\sum W_{A^{1}_{i}} A^{1}_{j} + \sum W_{A^{1}_{i}} D^{1}_{j} \right]$$

$$T^{1}_{A^{2}_{i}} = \frac{1}{\tau_{A^{1}_{2}}} + \sum W_{A^{2}_{i}} A^{1}_{j} + \sum W_{A^{2}_{i}} D^{1}_{j}$$

$$T^{2}_{A^{2}_{i}} = \frac{1}{\tau_{A^{0}_{2}}} + T^{1}_{A^{2}_{i}} + \sum W_{A^{2}_{i}} A^{2}_{j} + \sum W_{A^{2}_{i}} D^{2}_{j}$$

If we apply the linalization, the NLGETME23 will transform to a linear system. This new system is called LNLGETME23 and it has the form [24]

$$\frac{dP}{dt} = D\left[f\left(P\right)\right]_{P=P_o} P$$

Where the jacobian is equal to the sum of two matrixes

$$\left[Df\left(P\right)\right]_{P=P_o} = K + K'$$

and

$$K = \begin{bmatrix} \begin{matrix} -T_{D_1^1}^{D_1^1} & \cdots & W_{D_{N_D}^1}^{D_1^1} \\ \vdots & \ddots & \vdots \\ W_{D_1^1}^{D_{N_D}^1} & \cdots & -T_{D_{N_D}^1}^{D_{N_D}^1} \end{matrix} & \begin{matrix} W_{A_1^1}^{D_1^1} & \cdots & W_{A_{N_A}^1}^{D_1^1} \\ \vdots & \ddots & \vdots \\ W_{A_{N_1}^1}^{D_{N_D}^1} & \cdots & W_{A_{N_A}^1}^{D_{N_D}^1} \end{matrix} & \begin{matrix} 0 & \cdots & 0 \\ \vdots & \ddots & \vdots \\ 0 & \cdots & 0 \end{matrix} \\ \begin{matrix} W_{D_1^1}^{A_1^1} & \cdots & W_{D_{N_D}^1}^{A_1^1} \\ \vdots & \ddots & \vdots \\ W_{D_1^1}^{A_{N_A}^1} & \cdots & W_{D_{N_D}^1}^{A_{N_A}^1} \end{matrix} & \begin{matrix} -T_{A_1^1}^{A_1^1} & \cdots & W_{A_{N_A}^1}^{A_1^1} \\ \vdots & \ddots & \vdots \\ W_{A_1^1}^{A_{N_A}^1} & \cdots & -T_{A_{N_D}^1}^{A_{N_A}^1} \end{matrix} & \begin{matrix} W_{A_1^2}^{A_1^1} & \cdots & W_{A_{N_A}^2}^{A_1^1} \\ \vdots & \ddots & \vdots \\ W_{A_1^2}^{A_{N_A}^1} & \cdots & W_{A_{N_A}^2}^{A_{N_A}^1} \end{matrix} \\ \begin{matrix} 0 & \cdots & 0 \\ \vdots & \ddots & \vdots \\ 0 & \cdots & 0 \end{matrix} & \begin{matrix} 0 & \cdots & 0 \\ \vdots & \ddots & \vdots \\ 0 & \cdots & 0 \end{matrix} & \begin{matrix} -T_{A_1^2}^{A_1^2} & \cdots & \hat{W}_{A_{N_A}^2}^{A_1^2} \\ \vdots & \ddots & \vdots \\ \hat{W}_{A_1^2}^{A_{N_A}^2} & \cdots & -T_{A_{N_A}^2}^{A_{N_A}^2} \end{matrix} \end{bmatrix}$$

$$K' = \begin{bmatrix} \begin{matrix} 0 & \cdots & 0 \\ \vdots & \ddots & \vdots \\ 0 & \cdots & 0 \end{matrix} & \begin{matrix} \bigstar_{11} & \cdots & \bigstar_{1N_A} \\ \vdots & \ddots & \vdots \\ \bigstar_{N_D1} & \cdots & \bigstar_{N_DN_A} \end{matrix} & \begin{matrix} \square_{11} & \cdots & \square_{1NA} \\ \vdots & \ddots & \vdots \\ \square_{ND1} & \cdots & \square_{ND,NA} \end{matrix} \\ \begin{matrix} 0 & \cdots & 0 \\ \vdots & \ddots & \vdots \\ 0 & \cdots & 0 \end{matrix} & diag\left(\begin{bmatrix} \sum_{j=1}^{N_D} \blacktriangle_{1j} \\ \vdots \\ \sum_{j=1}^{N_D} \blacktriangle_{N_Aj} \end{bmatrix}\right) & diag\left(\begin{bmatrix} \sum_{j=1}^{N_D} W_{D_j^1}^{A_1^1} \\ \vdots \\ \sum_{j=1}^{N_D} W_{D_j^1}^{A_{NA}^1} \end{bmatrix}\right) \\ \begin{matrix} 0 & \cdots & 0 \\ \vdots & \ddots & \vdots \\ 0 & \cdots & 0 \end{matrix} & diag\left(\begin{bmatrix} \sum_{j=1}^{N_D} W_{D_j^1}^{A_1^2} \\ \vdots \\ \sum_{j=1}^{N_D} W_{D_j^1}^{A_{NA}^2} \end{bmatrix}\right) & diag\left(\begin{bmatrix} \sum_{j=1}^{N_D} W_{A_1^2}^{D_j^1} \\ \vdots \\ \sum_{j=1}^{N_D} W_{A_{N_A}^2}^{D_j^1} \end{bmatrix}\right) \end{bmatrix}$$

with

$$W_{A_i^2}^{A_i^1} = 0 \text{ for } i = 1..NA \qquad \square_{ij} = W_{D_i^1}^{A_j^1} - W_{A_j^2}^{D_i^1}$$

$$\bigstar_{ij} = W_{D_i^1}^{A_j^1} - W_{D_i^1}^{A_j^2} - W_{A_j^1}^{D_i^1} \qquad \blacktriangle_{ij} = W_{A_i^1}^{D_j^1} - W_{D_j^1}^{A_i^1}$$

The NLGETME23 is equal to NLGETME if all the terms related with the second levels are reject.

The NLGETME23 is equal to GETME if all the terms related with the second levels are reject and we considerate the resonant case.

References

[1] V. Lupei, A. Lupei, G. Boulon, “The effects of sensitisation on the activator emission in laser crystals,” J. Lumin. ’72-74, 948-950 (1997)

[2] V. Lupei, A. Lupei, “Emission dynamics of the 4F3/2 level of Nd3+ in YAG at low pump intensities,” Phys. Rev. B 61, 8087-8098 (2000).

[3] V. Lupei, A. Lupei, S. Georgescu, C. Ionescu, “Energy transfer between Nd3+ ions in YAG,” Opt. Commun. 60, 59-63, (1986).

[4] S. O. Vásquez, “Crystal model for energy-transfer processes in organized media: Higher-order electric multipolar interactions.” Phys. Rev. B 60, 8575 (1999).

[5] V. Ostrumov, T. Jensen, J.-P. Meyn, G. Huber, M. A. Noginov, "Study of luminescence concentration quenching and energy transfer upconversion in Nd-doped LaSc3(BO3)4 and GdVO4 laser crystals", J. Opt. Soc. Am. B 15, 1052-1060 (1998)

[6] Laser Operation,” IEEE J. Quantum Electron. 34, 2246-2255, (1998).

[7] J. Hegarty, D. L. Huber and W. M. Yen, "Fluorescence quenching by cross relaxation in LaF3:Pr3+, Phys. Rev. B 25, 5638-5644 (1982)

[8] E. Luria, S. R. Rotman, J. A. Mares, G. Boulon, A. Brenier, L. Lou, “Energy transfer between Vr3+ and Nd3+ in Cr,Nd: YAP,” J. I.umin. 72-74, 951-953 (1997)

[9] L. J. Dowell, Los Alamos National Laboratory report LA-11873-MS (1990).

[10] T. Forster, Ann. Phys. (Leipzig) 2, 55 (1948).

[11] L.A. Diaz-Torres, O. Barbosa-Garcia, C.W. Struck, R.A. McFarlane, “Analysis of experimental Nd3+ emission transients with fast sub-microsecond decay componentand a subsequent non-exponential long-term decay with Monte-Carlo simulations,” J. Lum. 78, 69 (1998).

[12] R. K. Watts, “Energy transfer phenomena,” in Optcal Properties of Ions in Solids, B. Di Bartolo, Ed. Plenum Press, New York and london (1975) p. 307.

[13] D. L. Dexter, “A theory of sensitized luminescence in solids,” J. Chem. Phys. 21, 836-850(1953).

[14] Richard C. Powell, *Physics of Solids-State Laser Materials* Springer (1998)

[15] L. F. Johnson and H. J. Guggenheim Infrared-Pumped Visible Laser Appl. Phys. Lett. 19 (2), 44–47 (1971).

[16] Y. K. Voron’ko, V. V. Osiko and I. A. Shcherbakov *Luminescence of Laser Crystals* Izvestiya Akademii Nuak SSR. Seria Fizicheskaya 46 (5), 970–978 (1982).

[17] M. Yokota and O. Tanimoto J. Phys. Soc. Japan 22, 779 (1967).

[18] A. I. Burshtein *Hopping Mechanism of Energy Transfer* Sov. Phys. LETP 35 (5), 882 (1972).

[19] V. Müller *Characterisierung und Optimierung von hochdotierten Yb:YAG* Laserkristallen Master’s thesis, Institute of Laser-Physics, University of Hamburg, Germany (2001).

[20] A. Bolz Energietransfer in Ytterbium-dotierten Sesquoxiden Master’s thesis, Institute of Laser-Physics, University of Hamburg, Germany (2001).

[21] J.T. Vega-Duran, L.A. Diaz-Torres, M.A. Menesses-Nava S.F. Mosiño “Exact solution to the general non-radiative energy transfer master equations in crystalline materials,” J. Lumin. 91, 233-241 (2000).

[22] O. Barbosa-Garcia, C. W. Struck, "Monte Carlo treatment of the nonradiative energy transfer process for nonrandom placements of dopants in solids,” J. Chem. Phys. 100, 4554,(1994),

[23] O. Barbosa-Garcia, R. A. McFarlane, M. Birnbaum and L. A. Diaz-Torres, “Neodymium-to-erbium nonradiative energy transfer and fast initial fluorescence decay of the 4F3/2 state of neodymium in garnet crystals,” J. Opt. Soc, Am. B14, 2731- 2734 (1997),

[24] Lawrence Perko, Differential Equations and Dynamical System, second Edition, ed Springer

Chapter 3

Yb^{3+} dimers as quenching centers in ZrO_2:Yb^{3+} nanocrystals.

1. Introduction

In Chapter 1 we have shown experimental evidence of the quenching for the IR Yb^{3+} emission in ZrO_2. It is also shown the visible emission that might become from the Yb dimers, and is known as the cooperative emission. There, we suggested that the Yb dimers could act as quenching centers, it means as acceptors, of the IR Yb^{3+} emission, donors emission. Thus, the cooperative emission corresponds to an upconversion process from the single Yb^{3+} ions to the Yb dimers. Revised and extended theoretical models for the no radiative energy transfer between two species of ions within a crystalline material were developed in Chapter 2. These new models are general and take in to account the most plausible off-resonance energy transfer conditions in real crystal phosphors. In the present Chapter we apply the above developed models to study the non radiative energy transfer processes responsible for the quenching of the IR Yb^{3+} emission in ZrO_2:Yb^{3+}. For that, we have to make a several considerations, the most important is that the Yb dimers are the acceptors or quenching centers.

2. The Yb dimers in ZrO2.

In crystalline $ZrO_2 : Yb^{3+}$ we only have one species ions: the Yb^{3+} donors. That is, the acceptor species initially doesn't exist. Now, if we introduce the pair concept, we are able to introduce a new species of "centers", which have three energy levels (see Chap 1). These new "centers" will play the role of the acceptor species. In section 1.5 we indicated that ZrO_2 presents three different crystalline structures or phases: monoclinic, tetragonal,

and cubic (see also Appendix B). The phase composition being determined by the Yb^{3+} dopant concentration. Now, the Zr ions occupy specific sites within the crystalline structure, and those are the sites in which the Yb ions can be substituted. See Appendix B for the Zr and O ion site coordinates and structures of ZrO_2. Then distances among Yb ions are constrained to be among the distances between Zr sites, and the discrete distribution of distances depends on the specific crystalline phase. Table I list the first eight neighbor distances for each of the crystalline phases of ZrO_2.

Tabla 1 first eight neighbor distances for each of the crystalline phases of ZrO_2

Neighbor distances	1	2	3	4	5	6	7	8
Cubic (Å)	3.631	5.135	6.2891	7.262	8.1191	8.8941	9.6067	10.27
Monoclinic(Å)	4.0064	4.0514	4.2897	4.3198	4.4669	4.5236	4.593	4.6777
Tetragonal(Å)	3.5925	3.6291	5.0806	5.1837	6.2436	6.3069	7.185	7.2583

In order to simulate a Yb doped ZrO_2 crystal, first we construct a crystal sample of size $(N_a a)$x$(N_b b)$x$(N_c c)$, where (a, b, c) are the unitary cell parameters (see appendix B), and N_a, N_b, N_c are integer numbers. Then, we can randomly substitute the Yb ions within the available Zr sites up to the desired Yb concentration. After that, we are in the position to compute the distances among all the Yb ions within the generated crystalline sample. Thus, we can start to construct the Yb dimers, by substituting two Yb ions, separated by a distance R_d from each other, by a single dimer located at the mean distance between the corresponding Yb ions, see Figure 1a,b. If figure 1c) we show the top view of a monolayer of Yb doped cubic Zirconia (Fig 1.d) of 7x6x1 unitary cells; yellow spheres are oxygen, navy blue are Zr, sky blue are substituted Yb, and lastly the ellipses represent dimers. It is also assumed that there always will be an Oxygen ion bridging the pair of Yb ions, that is supported in the fact that ZrO_2 is constituted only of Zr and O ions. That is, we consider that the crystalline samples do not have defects or Oxygen vacancies.

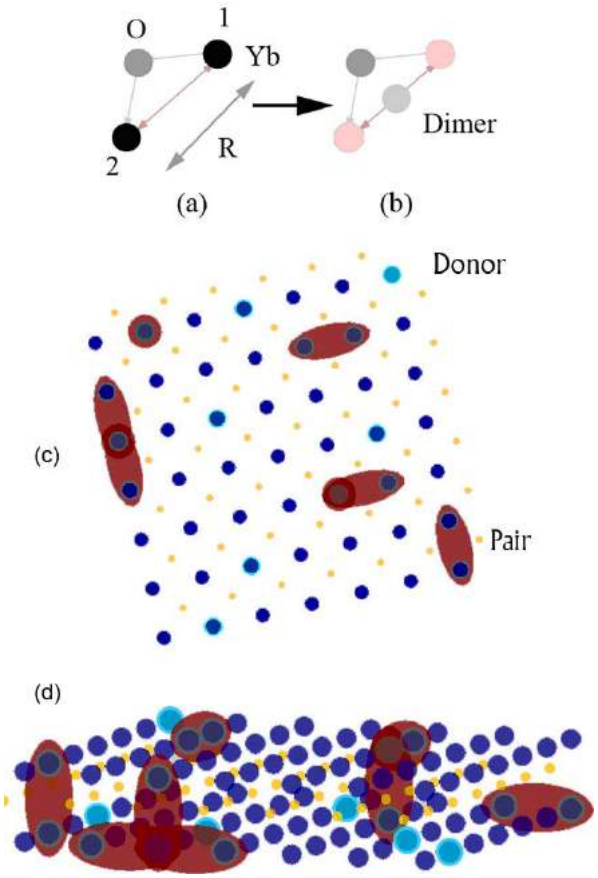

Figure 1. Some formation possibilities for the Yb dimers in Cubic Zirconia.

The Yb dimer construction results in a decrease of the net population of donor ions (single Yb^{3+} ions) and an increase of the acceptor Yb dimers. Such reduction on donor ions depends on the net Yb^{3+} concentration, that is, the higher the Yb^{3+} concentration the higher probability of having two Yb ions at a R_d distance one of the other. In addition, since the crystalline sample is finite, its size will constitute a constrain on the net number of dimers that can be formed for a fixed Yb^{3+} concentration. It is important to remember that donor (and acceptor as well) concentration is a macroscopic measure of the average number of donors per unit volume. So, in order to get a more realistic approach we sample the above procedure for a very high number of computer generated crystalline samples, and average the outcoming donor and acceptor concentrations over all the generated samples. For all

the calculations presented from now on we have considered that the dimer distance was equal to the first neighbor distance for each crystalline phase, that is R_d= 4.0064A, 3.5925A ,3.631A, for the monoclinic, tetragonal, and cubic phases of ZrO_2. The number of generated samples was always 1500 crystal samples. Of course it is expected that the donor (single Yb^{3+} ions) and acceptor (Yb dimers) concentrations also will have a dependence on the crystalline phase since the Zr sites coordinates and first neighbor distances are different for different crystalline phases, see appendix B. In the following we present the most representative results of having taken in to account the above Yd dimer construction.

2.1 Nanocrystal size and phase effect on Donor and acceptor concentration.

TEM images of all the synthetized Zirconia samples were taken on a transmission electron microscope JEOL 2010FEG with an accelerating voltage of 200 kV and a point to point resolution of 0.19 nm. See Figure 2 for an example of the obtained images for the 4mol% Yb sample. The observed particle sizes were between 50 and 100 nm, see appendix B. From the TEM images of all samples we find that the dopant concentration does not affect particle sizes. Nevertheless, our crystal simulation indicate that dopant concentration affect directly to the donor and acceptor densities, depending on nanocrystal size and crystalline phase.

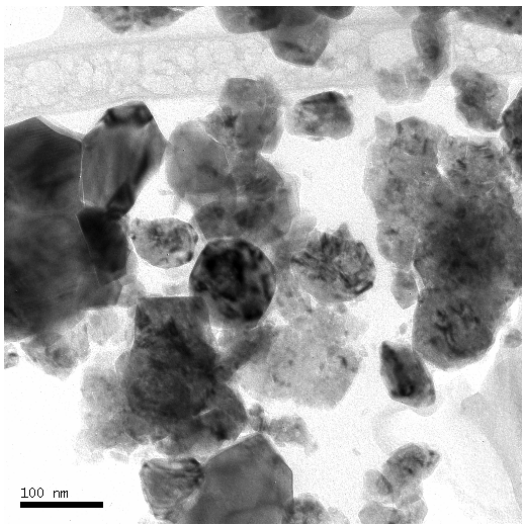

Figure 2 TEM image of a ZrO2:Yb^{3+} sample with 4%Yb^{3+}.

By doing the 2%mol Yb doped nanocrystals simulations for increasing size we computed the acceptor (Yb dimers in red) and donor (single Yb^{3+} ions in black) densities shown in Figure 4. Here the size is reported as the volume $V_{NC}=(N_a a)x(N_b b)x(N_c c)$ o the crystalline sample. It is also considered that $aN_a=bN_b=cN_c$, that is, the nanocrystalline samples are "cuasi cubic". Also in the forthcoming discussion when we refer to the Nanocrystal diameter (or size) we are considering that the diameter of the Nanocrystal is given by $\phi_{NC} = 1.24\sqrt[3]{V_{NC}}$. One can notice that both curves tend to saturation constant values as the nanocrystallite size increases, whereas the standard deviation of both densities tend to be zero (standard deviation bands are not shown in Fig. 3). These results indicate that as the nanocrystallite size increases the donor and acceptor densities tend to their corresponding bulk values. The bulk densities correspond to the macroscopic values that are the average of centers per unit volume under the assumption that the material extends over all space. From this, we consider that there is a cut off nanocrystal size for which it can be considered as "bulk particle". Meaning that for all particles of such size or higher the physical and optical properties will not change from the average value measured for macroscopic samples. From figure 3, one can note that for nanocrystals smaller than 10.77 nm, in average diameter size, it is a very important effect of the size on both donor and acceptor densities. That complex behavior depends also on the crystalline phase, and is quite different for the three different phase of Zirconia. It is very interesting to observe that for monoclinic phase the dimer concentration for small nanocrystals is higher that its presumed value for bulk particles.

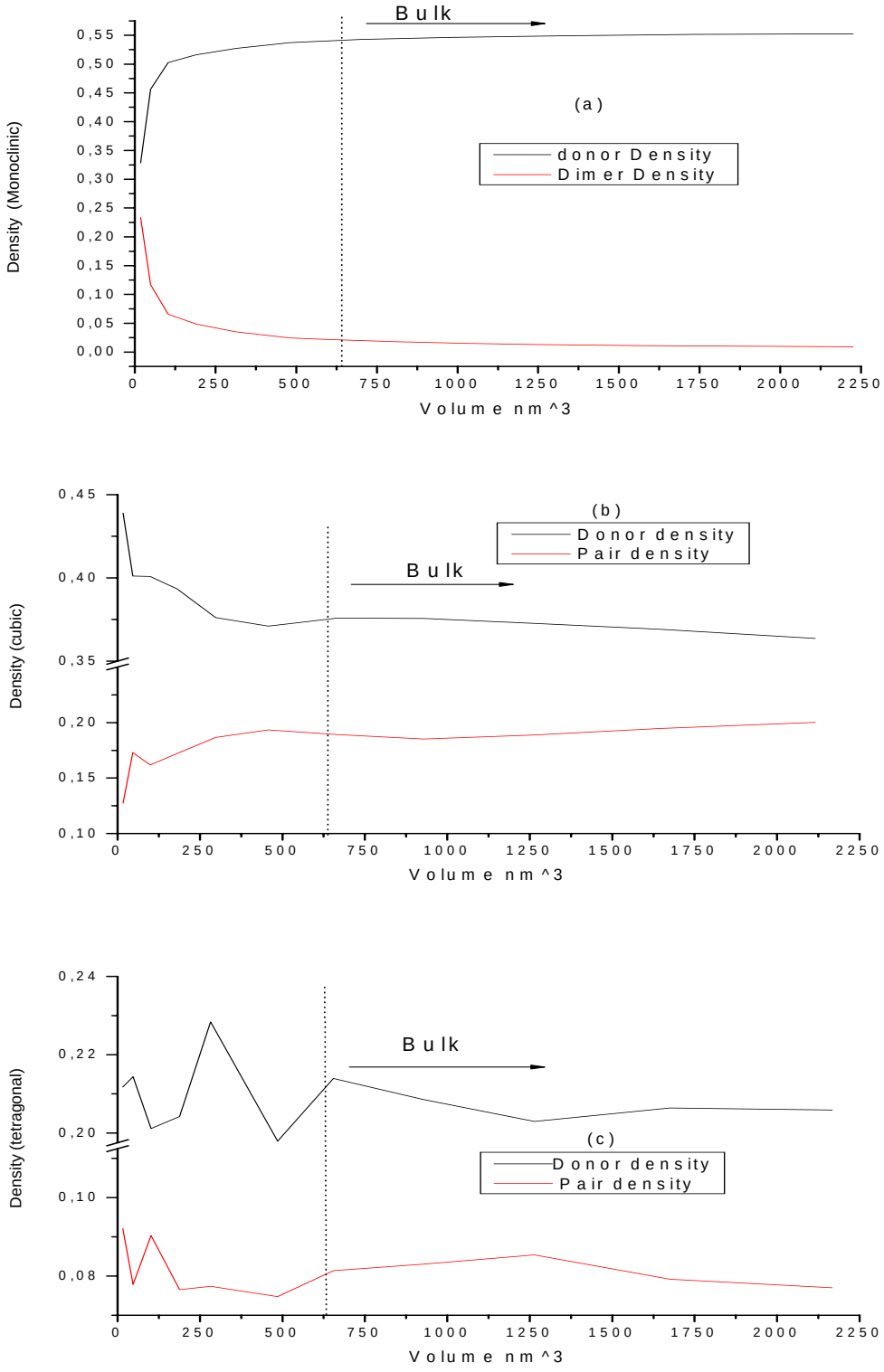

Figure 3 Donor (yb ions) and dimers density vs. volume (cubic diameter size, in unitary cells), for the a)monoclinic, b) cubic, and c) tetragonal phases of Zirconia doped with 2% Yb.

So, as a first approach, we considered that the bulk character starts at crystallites sizes where the corresponding saturation behaviors of the donor and acceptor densities start. That is, for particles with diameter sizes bigger that 10.77 nm (or a critical volume of 654.1 nm^3) approximately. Under this last consideration we have that our experimental measurements correspond to bulk like particles since our Zirconia particles are between 50 and 100 nm.

Another interesting result is show in the Figure 4 (we use only the cubic phase because this is the characteristic phase for a high Yb concentrations). The donor to dimer densities ratio exhibit a drastic reduction as the Yb concentration increases. This behavior could lead to the observed quenching in the IR Yb emission, since the overall amount donor density reduces and the dimer density increases as the Yb concentration increases. That is, we have more quenching centers and less IR emission centers as the Yb concentration increases.

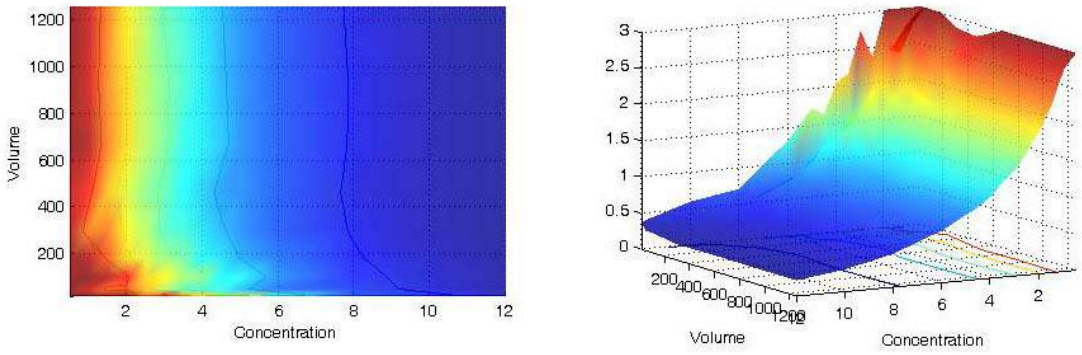

Figure 4 (Donor density) / (Pair density) decrease when we increase the Yb concentration. This behavior could be the reason of concentration quenching in IR emission.

2.2 Nanocrystal size effect on Donor effective Life time.

Up to now, we have defined a way to separate the dopant ions of a single species in two groups: Donors (isolated ions) and Acceptors (pairs or dimers). Assuming all these centers are excited at time t=0, by a laser pulse, the dynamics of the population of both type of centers could be described by the rate equation models developed in Chapter 2. That is, we

can predict the decay evolution of both the donors and acceptors under the influence of several possible energy transfer process among both subsystem centers. So in order to make one of such predictions we only have to evaluate GETME (or NLNGETME) as indicated in Apendix A, and the needed parameters are: the crystalline structure of the host, the coordinates of the crystallographic sites available to substitute the dopant ions, the concentration of dopant ions, the dimer distance R_d, the free ion donor and acceptor life times in absence of energy transfer τ_{D0} and τ_{A0}, and the free parameters for each of the assumed interactions among dopants: R_{0S}^{DA} with S=6,8,10 for the multipolar interactions, and R_0^{DA} and L^{DA} for the exchange interactions. The microscopic individual emissions are then calculated and averaged over a large number of numerically generated crystal samples according to Eq 14 in the Chapter 2. Then, the effective life time of each center (donor or acceptor) is obtained by integrating the predicted decay over the time window [0,T] used in the simulation:

$$\tau_{ef}^{D} = \int_0^T \phi_D(t)dt \quad \text{and} \quad \tau_{ef}^{A} = \int_0^T \phi_A(t)dt \qquad (1)$$

Since the number of acceptor dimers increases one expects that the overall energy transfer from donors to acceptors will increase, and therefore the quenching of the donor emission will increase. In fact, variations on the dimers acceptor density are traduced in variations on the quenching of the donor luminescence. That is, variations on the dimer acceptor density lead to variations on the effective life time of the donor luminescence. Since we have shown that size and phase are factors that affect the density of dimers it should be expected that variations in phase or crystallite size should lead to variations on the effective life time of the donor centers for fixed concentrations of dopants. That is, quenching or enhancement of the quantum efficiency ($\eta = \tau_{ef}^{D} / \tau_{D0}$) can depend on the crystallite size for a fixed concentration of a single dopant species, if the formation of pairs is taken in to account. Figure 5 shows the effective life time τ_{ef}^{D} of single Yb^{3+} ions (donors) as the crystallite size increases for two Yb^{3+} concentrations: (1) .5% Yb, (circles points) and (2) 4%Yb (square points). This calculation was done considering the corresponding phase

compositions reported in Apendix B. It was also considered that all the dimers were initially excited at the first level and that energy transfer from the donor to the dimers (up to its second excited level) was driven by a single dipole-dipole interaction with critical distance of R_{06}= 5.25 A. The pair distances R_d were the respective first neighbors distances for the corresponding crystallite phases reported in table I. It was assumed an off-resonance situation but with null back transfer and null migration processes. From the calculations shown in Fig. 5, on can observe that τ_{ef}^{D} has decreasing behavior as the crystallite size increases (reduction on the quantum efficiency). On the other hand, it seems clear that for sizes lager than 10.77 nm τ_{ef}^{D} tends to a limit value. We presume such value corresponds to the bulk value of τ_{ef}^{D}. It also can be observed that the variation trend of τ_{ef}^{D} depends on the crystallite phase, we can recall that for 1.5% Yb content the phase is a mixture of tetragonal and monoclinic whereas for 4% we have pure tetragonal phase. We can also observe the considerable decrease of τ_{ef}^{D} between 1.5% and 4% Yb content. That is an indicative of concentration quenching, where the only external parameters changing is the overall Yb concentration. That is the dimer and final donor densities are dependent on the Yb^{3+} concentration.

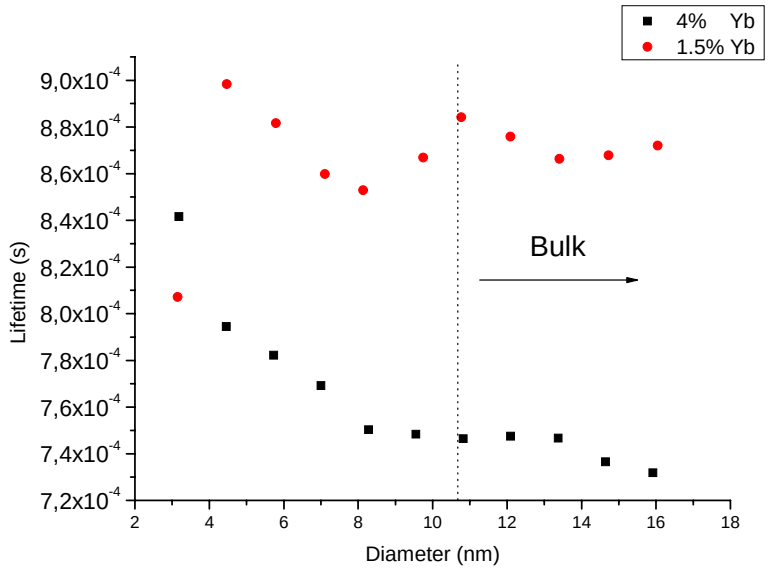

Figure 5 Size effect lifetime using GETME and we only considerate dipole-dipole interaction R_{06} = 5.25 A.

3. Quenching simulation of the IR emission of Yb^{3+} in ZrO_2

At last we are in the position to use the models developed in Chapter 2 to study the quenching of the IR emission of Yb^{3+}. What we do is to use model GETME or LNLGETME or NLGETUP in order to fit the experimental decays of the IR emission of Yb^{3+} in ZrO_2 shown in Chapter 1. That fitting allows us to determine the nature of the interactions responsible of the energy transfer process that lead to the observed quenching. For that, we have to make a couple of considerations:

1) The overall (nominal) concentration of Yb^{3+} ions is to be divided in to subsystems: a)The donors or isolated Yb^{3+} ions, and b) the acceptors or Yb-Yb pairs here so called Yb dimers.

2) It is considered by simplicity that at t=0 all Yb^{3+} ions are excited. That means that both the donors (single Yb^{3+} ions) and acceptors in its first energy level, are excited at t=0. That is, acceptors in its second energy level are not excited.

The second assumption also allows us to consider the energy transfer process as a process among two species of two level ions. That is we can use GETME or NLGETME. The drawback is that we will not be able to get predictions for the emission of the first and second energy levels of the dimers. That is, even when the models can compute the acceptors emissions, such predictions do not correspond to the real situation. That means we have the acceptors only as trap or sink centers for the IR emission of the donors (Yb^{3+} isolated ions).

Thus we calculated the donor emission for a direct energy transfer from the isolated Yb^{3+} ions to the dimers by evaluating the solution to the NLGETME, see appendix A for the calculation algorithm. For this calculation, Yb^{3+} ions are randomly placed at the corresponding ZrO_2 lattice sites within a numerically generated crystal sample of 10,77 nm of diameter. We use this diameter because the sizes of our phosphors were around 100 nm

for all Yb^{3+} concentrations. That is, we had bulk-like samples. After that the Yb dimers were computed by using the actual Yb^{3+} coordinates within the crystalline sample, and considering R_d equal to first neighbor distance corresponding to the crystallite phase composition for each Yb concentration (see Appendix B).

Then, with such crystal sample the transfer rates matrix (see matrix 48 in of chapter 2) among all dopants (in this case single Yb ions and Yb dimers) are calculated according to the assumed interaction that drives the transfer of energy. Since we pretend to simulate the quenching in the IR emission of the Yb^{3+} ions, we consider that exchange interaction doesn't exist and that the dipole-dipole interaction is the only one that drives the direct energy transfer between donors (Yb ions) to acceptors (Yb dimers). We solve the first order approximation LNLGETME (see eq. 50). The microscopic individual emissions are calculated and averaged over a large number of numerically generated crystal samples according to Eq 14 in the chapter 2.

Assuming that the dopant concentration should not alter the micro interaction parameter R_{0S}^{DA}, we find an adjustment using LNLGETME for all the concentrations under resonant conditions, see Figure 6. The all concentrations fitting parameter is the constant $R_{06} = 5.25A$. Such value allows fitting simultaneously the decay trend of the IR emission of Yb^{3+} for all the studied Yb^{3+} concentrations. That fact gives this value a character of physical constant for the direct energy transfer interaction from single Yb^{3+} ion to the Yb dimer, no matter which is the crystalline phase of ZrO_2 or the overall Yb concentration, or the crystallite size. That is, we have microscopic quantum characteristic interaction parameters that do not depend on the number of interacting donor-acceptor pairs or host environment.

On the other side, we also used the LNLGETME under off-resonance conditions, and find the results shown in Figure 7, for these simulations we use the same conditions that for simulations on-resonance (Fig. 6) but for back transfer it was now considered a value of $R_{06} = 6A$. These off resonance simulations do not adjust well for high concentrations, whereas they do for low Yb^{3+} concentrations.

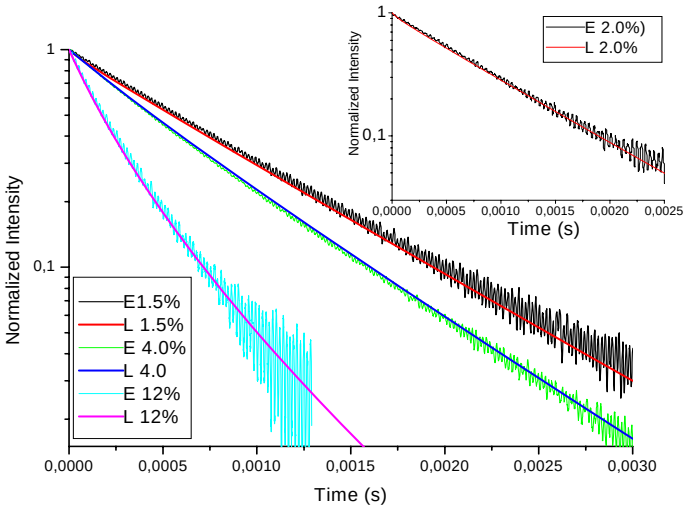

Figure 6. Concentration Quenching using LNLGETME on resonance conditions with R06 =5.25A. We have four Yb concentrations, 1.5%, 2%, 4% and 12%. The letter E means Experimental measurement and the letter L means the solution of GETME.

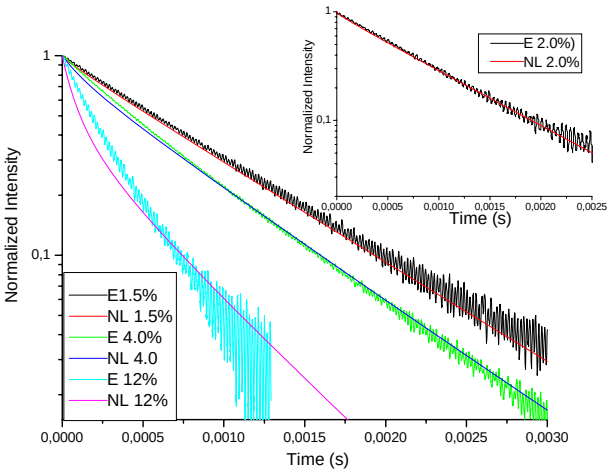

Figure 7. Concentration Quenching using LNLGETME for off-resonance conditions with R06 =5.25A fot direct transfer and R06=6.0A for back transfer.

Thus, from the results shown in Figures 6 and 7, it is clear that in fact the ZrO_2:Yb^{3+} is a system subject to resonant energy transfer, and that the quenching centers of the IR emission of Yb^{3+} are the Yb dimers. It was also shown that the density of dimers depends on the crystallite size and phase, in addition to its intrinsic dependence on the Yb^{3+} concentration. It was shown that a direct dipole-dipole driven energy transfer from the single Yb^{3+} ions to the Yb dimers is the mechanisms behind the quenching of the IR emission of the single Yb^{3+} ions. It was also determined a single interaction parameter for the interaction between single Yb ions and dimers that do not depends on the dopant concentration nor on the crystalline phase. The corresponding parameter value was R_{06}=5.25 $\dot{A}$ for a direct energy transfer process driven by a dipole-dipole interaction.

In regard of the observed visible emission no analysis work was done by now, but we are confident that the two to three energy level ions model developed in chapter 2 will be a good approximation. Unfortunately its numerical complexity do not allowed us to implement the algorithm on the current PC`s available at the moment. We hope in the near future to have PC`s with enough memory capacity to handle such modeling. We that became possible will be able not only to study the visible emission of the dimers, but also initiate the study of more complex systems were we can have more than one species of dopants. The first case could be the Yb to Er system, where we also will be able to consider the cooperative contributions of the dimers to the upconversion processes that lead to the upconversion emission of Er.

Chapter 4 Conclusions and Perspectives

4.1 Conclusions

We can form a pair, with two ions of Yb who are very closely; this pair has three levels of energy. A good approach is to consider that the pair will be positioned in the crystal host at the average distance between Yb ions. We have analyzed the fluorescent decay of Yb^{3+} ions in several co-doped ZrO_2 samples with the numerical solutions of the corresponding NLGETME. We can simulate the lifetime quenching as a function of the concentration. We use the pair approach to simulate the donor fluorescence decay in the $ZrO_2:Yb^{3+}$. To simulate the quenching of the IR emission of the Yb^{3+} ions, we consider that exchange interaction doesn't exist and that the dipole-dipole interaction is the only one that drives the direct energy transfer between donors (Yb ions) to acceptors (Yb dimers). We are able to adjust the experimental data of the decay of the fluorescence in the infrared emission using a unique interaction parameter. First we find an adjustment using LNLGETME on resonance conditions for all the Yb^{3+} concentrations. We adjust with a single R_{06} constant all the samples simultaneously and it was found to have a value of $R_{06} = 5.25\dot{A}$. That interaction parameter does not depend on the concentration of Yb, being thus a characteristic parameter of the direct energy transfer from Yb ions to Yb dimers. This indicates that it is a parameter that characterizes the decay of the IR fluorescence of Yb in ZrO_2:Yb, and leads to the quenching of such fluorescence through the consideration of dimer as acceptors. Such dimers are naturally formed (constructed) within the doped crystals by using the first neighbor distance as the distance that defines the Yb dimer. On the other side, when considering NLGETME on off-resonance conditions, we can adjust only for low Yb^{3+} concentrations with a unique back transfer parameter of $R_{06} = 6\dot{A}$. For higher concentrations, over 4% Yb3+ content, the off-resonance approach does not give a good fit to the experimental decays. That is presumed as a confirmation that the system single Yb3+ ions and Yb dimers in fact constitutes a system were the resonance conditions are naturally given by the definition of the dimer energy states.

Varying the crystallite size in a simulate way, it was found that both the donors density and dimer density are approximately constant for crystallite diameters superior to 10,77 nm. Then, for inferior diameters to 10,77 nm we have a nanocrystal and for superior diameters the material it expected to present bulk-like behavior. For a small diameter (<10.77 nm) the lifetime has a considerable size dependence, but the lifetime tend to be almost constant if the crystallite volume increase.

We can reproduce and predict the behavior of the lifetime and its dependence on dopant concentration, in particular for the IR emission of Yb^{3+} in $ZrO_2:Yb^{3+}$. So, our results support the assumption that Yb dimers are responsible of the concentration quenching for the IR Yb^{3+} emissions.

4.2 Perspectives

We will try to apply the NLGETUP to explain the lifetime quenching in the visible region (cooperative up conversion emission). For that we will have to deal with the two to three energy level scheme. On that scheme the upconversion superior levels appear naturally. If the model works for the Yb^{3+} system were the on-resonance is a fact, we can expect good results for more complicated systems where the off-resonance conditions are predominant. That is the case of upconversion processes in Yb to Er in many crystalline systems. In particular in our group there is experimental evidence of very efficient upconversion processes for Yb-Er codoped ZrO_2. Besides, it is important to verify if the first order approximation of NLGETUP works properly. If that is the case, we will be in the possibility of solve and simulate the lifetime quenching in the visible region for many systems were visible or cooperative emission are present.

Appendix A

Diagonalization

The algebraic technique of diagonalizing a square matrix K can be used to reduce the linear system

$$\dot{P} = KP \tag{A1}$$

to an uncoupled linear system. We first consider the case when K has real, distinct eigenvalues. The following theorem from linear algebra then allows us to solve the linear system 1.

Theorem 1. If the eigenvalues $\lambda_1, \lambda_2, ..., \lambda_n$ of an *nxn* matrix K (in our case $n = N_A + N_D$) are real and distinct, then any set of corresponding eigenvectors $\{v_1, v_2, ..., v_n\}$ forms a basis for R^n, the matrix $\Theta = [v_1, v_2, ..., v_n]$ is invertible and

$$\Theta^{-1}K = diag[\lambda_1, \lambda_2, ..., \lambda_n] \tag{A2}$$

in order to reduce the system 84 to an uncouple linear system using the above theorem, define the linear transformation of coordinates

$$\zeta = \Theta^{-1}P \tag{A3}$$

where is the invertible matrix defined in the theorem. Then

$$P = \zeta \tag{A4}$$

$$\dot{\zeta} = \Theta^{-1}\dot{P} = \Theta^{-1}KP = \Theta^{-1}K\zeta \tag{A5}$$

and, according to the above theorem, we obtain the uncoupled linear system

$$\dot{\zeta} = diag\left[\lambda_1, \lambda_2, ..., \lambda_n\right]\zeta \tag{A6}$$

This uncouple linear system has the solution

$$\zeta(t) = diag\left[\exp(\lambda_1 t), \exp(\lambda_2 t), ..., \exp(\lambda_n t)\right]\zeta(0) \tag{A7}$$

And then since $\zeta(0) = \Theta^{-1}P(0)$ and $P = \zeta$, it follows that 1 has the solution

$$P(t) = \Theta E(t)\Theta^{-1}P(0) \tag{A8}$$

where $E(t)$ is the diagonal matrix

$$E(t) = diag\left[\exp(\lambda_1 t), \exp(\lambda_2 t), ..., \exp(\lambda_n t)\right] \tag{A9}$$

Also we can solve the system using the exponential operator defined like

$$e^{Kt} = \sum_{k=0}^{\infty} \frac{K^k t^k}{k!} \tag{A10}$$

it follows that 84 has the solution

$$P(t) = e^{Kt}P(0) \tag{A11}$$

In our program we prefer to use the Digitalization method because in the exponential operator method we would have to delimit the series and this would cause that the method was approximate.

GETME and LNLGETME Algorithm

Our model computes the solution for the non-radiative Transfer master equations for crystalline materials based on the solution GETME and LNLGETME, we can resume it in four fundamental steps to obtain the temporal evolution of P(t).

1. Generate numerically the k-th crystalline sample with donor and acceptor ions in the corresponding crystalline places.

2. Calculate the individual transfer rates of each dopant in the k-th crystalline sample and to outline the GETME or LNLGETME for the k-th crystalline sample.

3. Solve the GETME or LNLGETME in the exact way for the ions in the k-th crystalline sample. And to obtain the mean values of the probabilities of each ions for the systems of donors and acceptors ions in the k-th crystalline sample.

4. Repeat the steps one to three for each k crystalline sample, and obtain the microscopic values of the mean probabilities of excitement, averaging over Nm crystalline samples.

1. First step

In order to generate a crystalline sample numerically we have to reply the unitary cell a finite number of times Ncu. Each unitary cell of the crystal this defined by means of their constant vectors of the crystalline lattice $\vec{a},\vec{b},\vec{c}$, as well as for the directors cosines α,β,γ. The ions that constitute the unitary cell of the crystal are located in very defined positions by means of their coordinates $\left(x_{si},y_{si},z_{si}\right)_{cu}$ inside the unitary cell. In general, let us consider that in each unitary cell have two different classes of places. A class of places sd that they can be occupied by the species of donating ions, and a second class of places sa that they can be occupied by the species of acceptors ions. Let us also consider that in the unitary cell have Nsd available places of the class sd, and Nsa available places of the class sa. Then, if we reply this unitary cell Ncu times, then we will have generated a crystalline sample with $Nsd \times Ncu$ available places for donors and NsaxNcu available places for acceptors.

Once we have built the crystalline sample, the following step consists on placing the dopant ions to the wanted concentrations. We assume that we want our dopant crystalline samples with concentrations nd and na of donors and acceptors ions, respectively. Then, since we have $Nsd \times Ncu \times (Nsa \times Ncu)$ available sites to receive the donors, then the numbers of donating Nd that we should place in the sample is

$$N_D = int\left(n_D \times \left(N_{sd} \times N_{cu}\right)\right) \tag{A12}$$

where int is the function that capture the entire part of the argument. In a similar way an

expression for the of N_A is the number of acceptors. Thus we proceed to place them aleatory among the available places.

In $ZrO_2 : Yb^{3+}$ we only have one type ions (Yb), ie the acceptor initially doesn't exist. But if we use the pair concept, we generate a new type of "center" who has three energy levels, this new "center" act as acceptor. All the distances are calculated between neighbouring donors ions, we replace the donors by a pair, where this distance is smaller to Rd, this pair be positioned in the half distance.

2. Second step

Once we have the N_A and N_D ions accommodated in their prospective places inside the crystal, we calculate the distances of among all the ions and we store them in a matrix, then we substitute in the equation 11 for GETME or 46 for LNLGETME, in order to find the characteristic transfer matrix for the k-th crystal sample.

3. Third step

We calculate the eigenvectors and the eigenvalues of W and we substitute in the equation A8 for each time point whiting the desired time range of experimental observation. .

4. Fourth step

Repeat the steps one to three for each Nm crystalline sample, and obtain the microscopic values of the mean probabilities of excitement, averaging over Nm crystalline samples.

References

[1] Lawrence Perko, Differential Equations and Dynamical System, second Edition, ed Springer

[2] J.T. Vega-Duran, L.A. Diaz-Torres, M.A. Menesses-Nava S.F. Mosiño "Exact solution to the general non-radiative energy transfer master equations in crystalline materials," J. Lumin. 91, 233-241 (2000).

Appendix B

Nanocrystals doped with .5, 1.5, 2, 4 and 12 mol% of Yb_2O_3 were prepared by the sol-gel method using ytterbium chloride at 99.99% purity. The crystalline structure and crystallite size of the samples was investigated by XRD. The crystalline phase of ZrO_2:Yb^{3+} nanophosphor it depends on the Yb concentration. For 2 mol% of Yb_2O_3, the main crystalline phase was tetragonal with a little content of monoclinic. Pure tetragonal and cubic phase was obtained for 4 and 8 mol% doped sample, respectively. The average particle size ~50 nm was obtained from XRD pattern using the Scherrer equation. Both crystalline size and crystallite structure were confirmed with TEM and HRTEM [4].

The coordinates of the different crystalline phases of the ZrO_2 are shown in the table 1 [1,2 and 3]. The Yb dopant substitutes the Zr ions within the crystalline lattices.

Table 1 Coordinates of the ions inside the unitary cell.

	Crystal Coordinates Unitary cell								
	Cubic phase			**Monoclinic phase**			**Tetragonal phase**		
	a	**b**	**c**	**a**	**b**	**c**	**a**	**b**	**c**
Zr	0.00	0.00	0.00	0.274	0.038	0.209	0.0	0.0	0.500
Zr	0.00	0.50	0.50	0.725	0.538	0.290	0.5	0.5	0.000
Zr	0.50	0.00	0.50	0.725	0.961	0.790			
Zr	0.50	0.50	0.00	0.274	0.461	0.709			
O	0.25	0.25	0.25	0.937	0.828	0.152	0.0	0.5	0.954
O	0.75	0.75	0.25	0.937	0.671	0.652	0.0	0.5	0.454
O	0.75	0.25	0.75	0.063	0.171	0.847	0.5	0.0	0.545
O	0.25	0.75	0.75	0.550	0.254	0.017	0.5	0.0	0.045
O	0.25	0.25	0.75	0.550	0.245	0.517			
O	0.75	0.75	0.75	0.449	0.745	0.982			
O	0.25	0.75	0.25	0.063	0.328	0.347			
O	0.75	0.25	0.25	0.449	0.482	0.754			

Tabla 2 Lattice parameters

	a (Å)	b (Å)	c (Å)	α	β	γ
Cubic	5.135	5.135	5.135	90	90	90
Monoclinic	5.1507	5.2028	5.3156	90	99.196	90
Tetragonal	3.5925	3.5925	5.1837	90	90	90

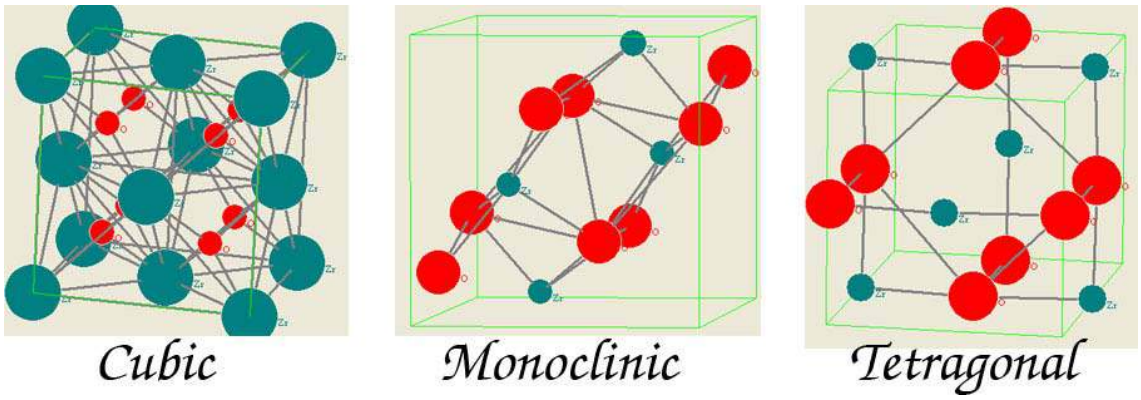

Figure 1 Crystalline lattice of ZrO_2 in the cubic, Monoclinic and tetragonal phase**.**

The phase concentration used in the simulation for different Yb% samples are show in the table 1.

Table 3 Phase concentration used in the simulation [4,5]

Yb concentration	**Cubic**	**monoclinic**	**tetragonal**
1.5% *	-	3%	97%
2.0%	-	3%	97%
4.0 %	100%	-	-
12%	100%	-	-

** For 1.5% we don't have the Phase concentration reported and we use the near Phase concentration (2%)*

NOTES

The table 1 is very important because this indicate the possible positions of donors ions (Yb). Our algorithm can consider the different crystals phases. We think that inside the nanocrystal different separate phases exist (figure 2).

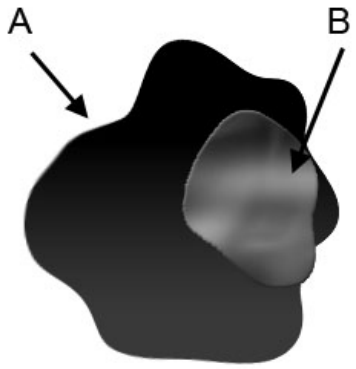

Figure 2, Nanocrystal with two phases A and B

For example, we have a nanocrystal with Pa percent of A phase and PB percent of B phase, the macroscopic fluorescence is given by

$$\phi_t = \frac{PA\phi_A + PB\phi_B}{100}$$

Where ϕ_A is the macroscopic fluorescence of the region with A phase inside of the nanocrystal and ϕ_B is the macroscopic fluorescence of the region with B.

References

[1] Wang, D.-N.;Guo, Y.-Q.;Liang, K.-M.;Tao, K. *Crystal structure of zirconium by Rietveld refinement* Science in China (1999), 42(1), 80-86

[2] Howard, C.J.;Kisi, E.H.;Roberts, R.B.;Hill, R.J. *Journal of the American Ceramic Society* (1990), 73(10), 2828-2833

[3] Hann, R.E.;Suitch, P.R.;Pentecost, J.L. *Journal of the American Ceramic Society* (1985), 68, 285-286

[4] E. De la Rosa*, D. Solis, L.A. Diaz-Torres, P. Salas, C. Angeles-Chavez, O. Meza

Blue-green emission in $ZrO_2:Yb^{3+}$ nanocrystals

[5] E. De la Rosa, P. Salas, L. A. Diaz-Torres, *Strong Visible Cooperative Up-Conversion Emission in $ZrO_2:Yb^{3+}$ nanocrystals.* Journal Nonoscience and Nanotechonlogy Vol. 5,1480-1486, 2005